FATIGUE AND CRACK PROPAGATION ANALYSIS OF A 11000 SHP TURBOPROP ENGINE FRONT BEARING STRUCTURE AND VALIDATION

11000 SHPLİK BİR TURBOPROP MOTORUN ÖN YATAKLAMA YAPISINDA YORULMA VE ÇATLAK BÜYÜME ANALİZLERİ VE VALİDASYONU

AYŞEGÜL YAMANER

PROF. DR. BORA YILDIRIM

Supervisor

Submitted to Institute of Sciences of Hacettepe University
as a Partial Fulfillment to the Requirements
for the Award of the Degree of Master of Sciences in Mechanical Engineering

2015

This work named "**Fatigue and Crack Propagation Analysis of a 11000 SHP Turboprop Engine Front Bearing Structure and Validation**" has been approved as a thesis for the degree of **MASTER OF SCIENCES IN MECHANICAL ENGINEERING** by the Committee Members below.

Prof. Dr Bora YILDIRIM
Head (Supervisor)   ………………………...........

Assoc. Prof. Dr. Benat KOÇKAR
Member   ………………………...........

Assoc. Prof. Dr. Şule Ergün
Member   ………………………...........

This thesis has been approved as a thesis for the degree **of MASTER OF SCIENCES IN MECHANICAL ENGINEERING** by Board of Directors of the Institute for Graduate School of Science and Engineering.

Prof. Dr. Fatma SEVİN DÜZ

Director of the Institute of
Graduate School of Science and Engineering

To my dearest family,

ETHICS

In this thesis study, prepared in accordance with the spelling rules of Graduate School of Science and Engineering of Hacettepe University,

I declare that

- all the information and documents have been obtained in the base of the academic rules
- all audio-visual and written information and results have been presented according to the rules of scientific ethics
- in case of using others Works, related studies have been cited in accordance with the scientific standards
- all cited studies have been fully referenced
- I did not do any distortion in the data set
- and any part of this thesis has not been presented as another thesis study at this or any other university.

29/06/2015

AYŞEGÜL YAMANER

ABSTRACT

FATIGUE AND CRACK PROPAGATION ANALYSIS OF A 11000 SHP TURBOPROP ENGINE FRONT BEARING STRUCTURE AND VALIDATION

AYŞEGÜL YAMANER

Master of Science, Department of Mechanical Engineering

Supervisor: Prof. Dr. BORA YILDIRIM

June 2015, 85 Page

All the components on a gas turbine should meet the requirements defined by the responsible associations. The front bearing structure which is assigned to be on the main load path of the engine has low cycle fatigue requirement to assure the integrity. Any invisible flaws or defects on the surface can cause cracks on the part. In this thesis, subjected component is investigated in the means of crack initiation and crack growth by the help of finite element method (FEM). Static structural FE analyses are completed prior to life calculations. Life number of cycles required to reach the failing limit is evaluated. A crack is introduced into FE model to find the crack growth rate. J-integral which is accepted as a fracture criteria and stress intensity factors are evaluated with respect to various defined crack lengths. Crack growth on the component is validated via LCF test. Test rig setup specifications and test results are also given. The finite element study delivered with a commercial software ANSYS / ANSYS Workbench version 16.0 and test results are compared in the study.

Keywords: finite element method, crack propagation, ANSYS, J-integral, stress intensity factors, crack growth rate, constant amplitude crack growth, crack modeling, front bearing structure, LCF

ÖZET

11000 SHPLİK BİR TURBOPROP MOTORUN ÖN YATAKLAMA YAPISINDA YORULMA VE ÇATLAK BÜYÜME ANALİZLERİ VE VALİDASYONU

AYŞEGÜL YAMANER

Yüksek Lisans, Makina Mühendisliği Bölümü

Tez Danışmanı: Prof. Dr. BORA YILDIRIM

Haziran 2015, 85 Sayfa

Gaz türbinleri üzerinde bulunan bütün parçalar için, sorumlu kurumlar tarafından gereklilikler belirlenmiştir. Bütünlüğü sağlamak için motorun ana yük yolu üzerinde bulunan ön yataklama parçasının, düşük çevrimli yorgunluk koşullarını sağlaması istenmiştir. Parça üzerindeki gözle görülemeyecek kadar küçük hatalar, parçada yıkıcı sonuçlar oluşturabilir. Bu çalışmada, sonlu elemanlar methodunun yardımı ile, ilgili komponent üzerinde çatlak başlaması ve büyümesi incelenmiştir. Ömür analizleri öncesinde statik yapısal analizler tamamlanmıştır. Çatlak katastrofik sona ulaşana kadar gereken toplam çevrim sayısı hesaplanmıştır. İlgili büyüme hızını bulmak için, sonlu elemanlar modeline bir çatlak eklenmiştir. Değişik çatlak uzunlukları için, kırılma kriteri olarak kabul edilen J-integral ve gerilme şiddeti faktörleri bulunmuştur. Komponent üzerindeki çatlak büyümesi, düşük çevrimli yorgunluk testi ile doğrulanmıştır. Çalışma içerisinde, test düzeneği özellikleri ve test sonuçları da verilmiştir. Sonuçta, ANSYS ve ANSYS Workbench versiyon 16.0 kullanılarak gerçekleştirilen sonlu elemanlar çalışması ve test sonuçları karşılaştırılmıştır.

Anahtar Kelimeler: sonlu elemanlar methodu, çatlak büyümesi, ANSYS, J-integral, gerilme şiddeti faktörü, çatlak büyümesi hızı, sabit genlikte çatlak büyümesi, çatlak büyümesi, ön yataklama yapısı, düşük çevrimli yorgunluk

ACKNOWLEDGEMENTS

I would like to sincerely thank to my supervising professor Dr. Bora Yıldırım for his guidance, support and encouragement throughout my research in every aspect. My gratitude goes to the committee members: Dr. Benat Koçkar and Dr. Şule Ergün.

For mentoring and guidance to gain experience, special thanks to Bilkay Gülaçtı and Mithat Murat Yalçın who were always there.

Most of all, thanks to my family and Ekin Çelik who made this study possible with their love, support and faith in me. Also, for their endless patience and support, I am grateful and thankful to my friends.

CONTENTS

SYMBOLS AND ABBREVIATIONS

Symbols

K_I	Stress Intensity Factor Mode-I
σ	Normal Stress
$\sigma_x, \sigma_y, \sigma_z$	Normal Stresses on planes x, y, z
F	Normal Force
A	Area, Amplitude Ratio
T	Shear Stress
L, l	Length
ε, e	Strain
ε_t	True Strain
$\varepsilon_e, \varepsilon_n$	Engineering, Nominal Strain
E	Young's Modulus
v	Poisson's Ratio
l_1, l_2, l_3	Principal Axes
$\sigma_1, \sigma_2, \sigma_3$	Principal Stresses
σ_m	Mean Stress
σ_a	Alternating Stress
$\sigma_{min}, \sigma_{max}$	Min, Max Stress
$\Delta\sigma$	Stress Range
R	Stress Ratio
S	Nominal Stress, Surface
N	Number of Cycles
$\Delta\varepsilon, \varepsilon_f$, b, c	Strain-Life Parameters
N_f, σ_f	Cyclic Stress-Strain Parameters
a	Crack Length
ΔK	Stress Intensity Factor Range
C, m	Paris' Law Parameters
K_{th}	Threshold of Stress Intensity Factor
K_c	Critical Stress Intensity Factor
Y	Parameter of The Geometry
a_0, a_c	Initial, Critical Crack Lengths
T_k	Traction

ω	Elastic Strain Energy
T_i	Traction Vector
Σ	Closed Surface
r_{ij}	Rotation Tensor
J	J-integral
Π	Potential Energy
Γ	Closed Surface Boundary
K_{Ic}	Fracture Toughness
J_{Ic}	Plastic-Elastic Fracture Toughness
G	Energy Release Rate
S_y	Yield Strength
M_x, M_y, M_z	Bending Moments
U	Deformation
S_1	First Principal Stress
S_{eqv}	Equivalent Stress
J_c	Critical J-integral Value
K_{eff}	Effective Stress Intensity Factor
K_{II}, K_{III}	Stress Intensity Factors Mode-II, III

Abbreviations

SHP	Shaft Horse Power
RPM	Revolutions per Minute
LCF	Low Cycle Fatigue
FPI	Fluorescent Penetrant Inspection
FBS	Front Bearing Structure
ASTM	American Society for Testing and Materials
S-N	Nominal Stress - Number of Cycles
HCF	High Cycle Fatigue
FEA	Finite Element Analysis
FE	Finite Element
Ti 6-4	Ti-6V-4Al
EPFM	Elastic-Plastic Fracture Mechanics
Ansys	Ansys Classic FE Software

Ansys WB	Ansys Workbench FE Software
CT	Central Tube
FF	Front Frame
PGB	Propeller Gear Box
IPC	Intermediate Pressure Compressor
IGV	Inlet Guide Vanes
UTS	Ultimate Tensile Strength
CAD	Computer Aided Design
HEX	Brick Elements in FEM
TET	Tetrahedron Elements in FEM
STBD	Starboard
DOF	Degree of Freedom
BRG	Bearing
SG	Strain Gauges

1 INTRODUCTION

1.1 Gas Turbines and Components

A gas turbine is defined as "*The power plant, which produces a great amount of energy for its size and weight.*" [1] Hence, it has found increasing service day by day in the power industry. In gas turbine industry, the aerospace engines lead in most of the technology developed. It is stated as "*The design criteria for these engines was high reliability, high performance, with many starts and flexible operation throughout the flight envelope.*" [1]

To achieve that, in last century, different types of gas turbine engines are developed to empower the aircrafts like turbojets, turbo shafts, turboprops etc. All are built around the knowledge of gas turbines. Aircraft engine manufacturers are in a race because of the limits of the market. Hence, development is driven by the need to reach more powerful but less consumable engines.
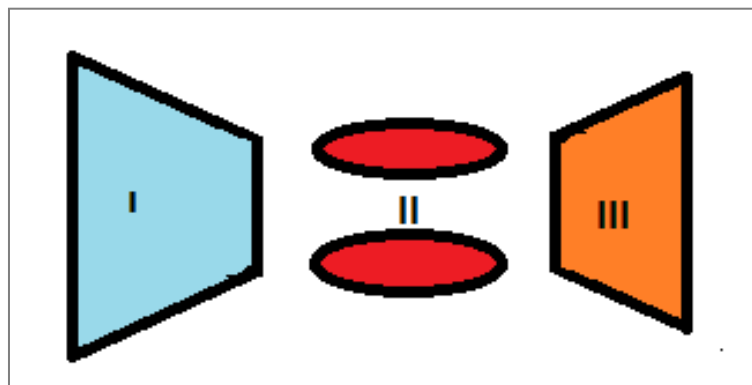

Fig 1.1 Main components of a gas turbine engine

As similar to all gas turbines it contains three main modules as shown in Fig 1.1;

   I.   *A compressor* which lets the air in and compresses,

  II.   *A combustion chamber*, which gets the high pressure air in and combust the fuel with it, and

 III.   *A turbine*, which is driven by the exhaust gases and drives the compressor.

1.2 Turbine Engines in Aviation

This part is reserved for a further look on types, advantages/disadvantages, general knowledge of gas turbine engines used in aviation:

a. Turbojet Engines: These are the simplest type of gas turbines. The sucked air by the compressor is compressed to get high pressured air. In combustion chamber,

high pressurized air is mixed with fuel and the mixture is burned. It comes to the turbine with high energy. The gases which contain high energy hit the turbine blades and make it spin. Finally the turbine energy is used to spin the compressor. The hot gases which pass the turbine cause propulsion in nozzle. Diagram of a typical gas turbine jet engine is shown in Fig 1.2. Turbojet engines are generally used military planes and rockets which need high speed and performance while they are not preferred in commercial planes because of their high fuel consumption.

b. Turbofan Engines: These type of engines are the most common in civil aviation. A turbofan engine basically uses a turbojet engine as a core engine by adding a fan in front of it. The fan sucks extra air which is not burned as named bypass air in a path which passes through out of the core engine. The fan is driven by an extra module named as Low Pressure Turbine. Generally, not only turbofan engines are more economical and efficient in lower speeds but also their specific fuel consumption is less than turbojets. A typical turbofan engine is shown in Fig 1.3

c. Turboprop Engines: Turboprop engines are the type whose turbine drives also a propeller which creates thrust. Since most of the energy of the exhaust gases are used to drive the propeller, unlike a turbojet engine they do not contain enough energy to create high thrust. The thrust is provided by exhaust gases is nearly 5%. The turbine is connected to the propeller through a reduction gear which converts high speed (RPM) but low torque power to low speed but high torque. A cross section of a turboprop engine is shown below as example, Fig 1.4. They are efficient in slow speed flights (max mach 0.7) and generally used on cargo planes.

d. Turbo shaft Engines: They are similar with turboprop engines in the meaning of having a propeller. They are not also used in high speeds but they are efficient in slow speed applications. They are generally used in helicopters. A typical engine diagram is shown in Fig 1.5.
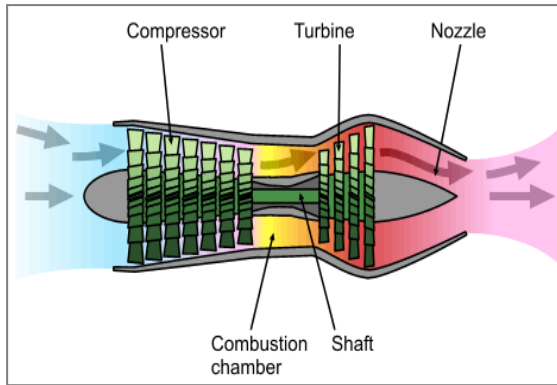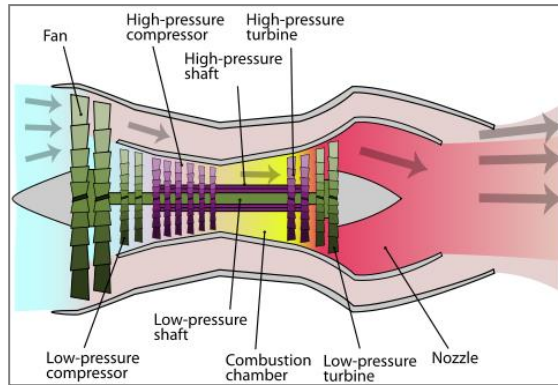
Fig 1.2 Diagram of a turbojet engine
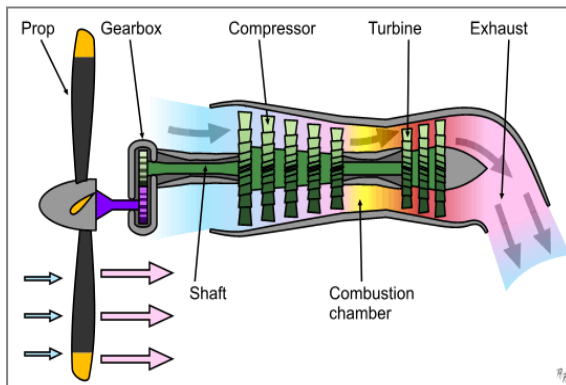

Fig 1.3 Diagram of a turbofan engine
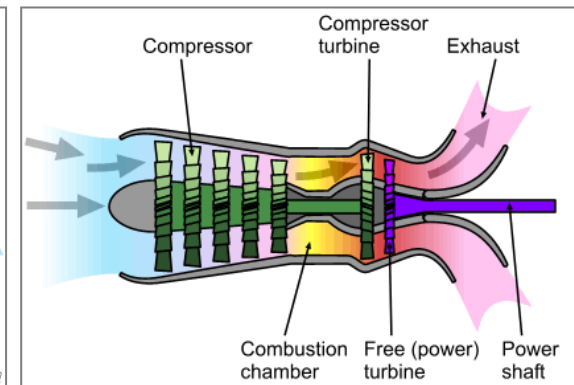

Fig 1.4 Diagram of a turboprop engine

Fig 1.5 Diagram of a turbo shaft engine

In this study, the subjected part named as Front Bearing Structure is a part of a turboprop engine which provides nearly 11000 shp to propeller.

1.3 Purpose of the Study

Every aircraft engine should be certified to be used on a plane. Every single part of the engine has different requirements. One of the most important requirements is life limitation. While some parts do not need this limitation like bolts and nuts because of having standards to use and being replaced in each service, other manufactured parts by the engine manufacturer need it either to complete the flights till the next service or at least for caution.

Critical components of the engine do not matter rotating or structural is subjected to high loads. It is necessary to monitor the life usage of these components and retire them from service before reaching the predicted life cycle to avoid any risk of catastrophic failure. The main failure mechanisms affecting the critical components of a gas turbine engine can is listed as "*low cycle fatigue, high cycle fatigue, thermo-mechanical fatigue, creep, overstress, corrosion, erosion, fretting and wear.*" [2]

Resisting capability of a part to the effects of these failure mechanisms depend on the material properties, design and operating environment. These factors which directly impact the life usage of the component are fixed by design and application of the engine such as the chosen engine cycle, its configuration and operating environment. Besides these factors, life usage may be affected by external factors like manufacturing and material defects, building and maintenance errors, foreign object damage and exceeding limits. But the external factors are assumed as avoidable by the control of the engine manufacturers, operators and maintainers.

Between these failure mechanisms, the LCF is concerned in this study which is the most common. Some components like all rotating parts, besides having life limits have limitations as no crack is allowed, not even initiation. But for some structural parts, non-rotating parts, crack initiation is allowed to reach the life limitation under the circumstances that propagation is assumed it would stop and not cause a failure.

Cracks can occur because of repeated loading where the highest principle stress is seen as well as caused by a defect coming from manufacturing processes or further raw material production like casting. After manufacturing processes, every part is inspected visually and with FPI. The tolerances for acceptance are different for each part. While higher limits are appropriate for structural parts, rotating parts are eliminated due to smallest defects in magnitude of microns.

Designed FBS should meet life limits as well as other parts. But since, it is a static component not rotating, it is allowed that can have crack on it but the crack can not propagate to cause a failure. In case of having a crack occurred because of repeated loading, it should not grow fast and at some point it should stop.

Even finite element modeling and hand calculations are realistic and proper for the design; certification requires component tests which will validate the finite element model and calculations besides engine tests. This procedure is followed for FBS also, validating the design and analysis by real stage tests.

This study is based on finite element analysis. Static strength is checked via static structural analysis, then fatigue analysis is performed to predict the life for the component and crack is implemented on the model to monitor the fracture criteria, J-integral along the changes in crack length. After defining the crack growth region, K_I values are evaluated and used to find the number of cycles needed for definite crack

lengths. The LCF fatigue test related to the component is appended which mainly helped to define crack sizes. Also, the results are compared between the analysis and the test in conclusion.

2 THEORETICAL BACKGROUND OF THE STUDY

In this study, a component will be used on a turboprop engine is selected and related analyses for its structural integrity are kept in view. Firstly, static strength analysis is performed just to verify the FE model is appropriate for fatigue and crack propagation analysis. Then, stress-life methodology is introduced to estimate the fatigue life of the hardware. Further, crack is assumed to be initiated and crack propagation analyses are performed. During the propagation of the crack, stress intensity factor K_I and J-integral values on the tip of the crack are tracked.

In this chapter, fundamentals of mechanics are reminded to be helpful with the static analyses' results. Afterwards, fatigue phenomena and comparison of life estimation methods are explained, in details stress-life methodology is stated. Finally, basics of fracture mechanics are recollected, fatigue crack propagation method under constant amplitude loading is stated for Region-II and a failure criterion based on J-integral is introduced in details. Also, a brief history of the finite element methodology which will lead this study is appended.

2.1 Structural Integrity of Design

Objective of the structural integrity is preventing catastrophic failures within the operational life of the part. It is assured via two main requirements; static strength and service life.

Static strength requirement assures the load carrying capacity of the hardware is enough for the max load applied in one load cycle. It can be verified via test during the design with nominal material properties and nominal dimensions of the geometry. But even it seems appropriate, static strength tests do not verify the load carrying capacity of the hardware with an initial damage and/or accumulated damage with usage.

Hence, service life requirements which are based on usage time or induced damage mechanisms during usage are involved. It defines not only the rate of damage accumulation but also the residual strength of the part. The service life testing basically defines a safe interval of operation with multiple intervention opportunities to minimize a catastrophic failure in service. [3]

2.2 Concepts of Mechanical Behavior of Materials

The basic terms of mechanics of materials are defined and basic formulations related to these terms are reminded in this part.

Mechanical behavior is defined as response of materials to forces in [4].This response can be deformation as well as a fail. The factors cause either deformation or fail are different. In this part, all definitions and factors should be considered in the meaning of deformation.

Strength is the property to define resistance capability of a material or a mechanical element under loading. But the limits in this concept is not definite, either stress required to deformation or fail [4]. It is best defined as "Strengths are the magnitudes of stresses at which something of interest occurs, such as the proportional limit, 0.2 percent-offset yielding, or fracture. In many cases, such events represent the stress level at which loss of function occurs." [5]

Stress concept can be stated as follows. In a tensile strength test machine, when a specimen is exposed to loading, the specimen will show a tendency to stretch, breaking the internal bonds. This breaking tendency is opposed by internal reactions, called stresses. [6] The resistance is uniformly distributed over the normal section and *normal stress; σ* is defined as this resistance per unit area, (2.3).

$$\sum F = 0 \tag{2.1}$$

$$F - \sigma A = 0 \tag{2.2}$$

$$\sigma = \frac{F}{A} \tag{2.3}$$

While normal stress occurs when the acted force is in the direction to the normal of the area, with *shear stress* the force acted is parallel to the area.

Two subscripts are required to define a stress; since the first subscript denotes the normal direction to the force acted areas; second subscript defines the direction of the acted force. Repeated subscripts denotes the normal stresses, whereas mixed ones used for shear stresses which can be also denoted as, *T*. The tensor notation is shown in (2.4).

$$\sigma_{ij} = \begin{vmatrix} \sigma_{xx} & \sigma_{yx} & \sigma_{zx} \\ \sigma_{xy} & \sigma_{yy} & \sigma_{zy} \\ \sigma_{xz} & \sigma_{yz} & \sigma_{zz} \end{vmatrix} \tag{2.4}$$

On the specimen of the tensile test machine mentioned in definition of stress, it is seen that the length of the specimen is getting longer when the applied force, F increases. For the increase dF, the length l, increases by dl. The normalized increase in length is given in (2.5).

$$d\varepsilon = \frac{dl}{l} \tag{2.5}$$

Integrating from the initial length, L_o, to the current length, L, gives the finite form which is called *true strain*, (2.6).

$$\varepsilon = \int dL \, / \, L = \ln(L/L_o) \tag{2.6}$$

In many applications of engineering, a simpler form called *engineering (nominal) strain* is used. It is defined as:

$$\varepsilon_n = \varepsilon_e = \frac{\Delta l}{l_0} = \frac{l_1}{l_0} - 1. \tag{2.7}$$

$$e = \Delta L \, / \, Lo \tag{2.8}$$

During elastic deformation, for small strains, as in metals which rarely exceed 0.005, engineering and true strains are nearly same. However, during plastic deformation, the difference between true and engineering strain gets higher. The relation between engineering and true strains for elastic deformation is given in (2.9).

$$\varepsilon t = \ln(1 + \varepsilon_e). \tag{2.9}$$

For metals, the stress and strain can be assumed to be proportional in the elastic region which is defined as Hookian solids. In 1678, Robert Hooke had performed experiments about stress and strain proportionality, later which is called Hooke's Law and the most simplified form of the law is shown in (2.10)

$$E = \frac{\sigma}{\varepsilon} \tag{2.10}$$

where E is called as Young's Modulus. It is derived from first principles and it depends on mainly the composition, crystal structure and nature of the bonding of elements. Even it is very limited, heat and mechanical treatments may affect the value of the Young's modulus.

Under uni-axial tension, in the direction that the force applied, the proportion between the stress and strain gives Young's modulus. Uni-axial tension also causes lateral strains denoted as in (2.11). Poisson's ratio, v, shows the intention of an isotropic solid to shrink in two directions, when it is sustained under the force applied in the third direction. Under a general stress state (σ_x, σ_y, σ_z) which produces the strain e_x, Poisson contractions of σ_y and σ_z can be shown as (2.12), while stress σ_x causes a contribution like (2.13).

$$e_x = e_z = -ve_x \tag{2.11}$$

$$e_x = -v\sigma_y /E \quad \text{and} \quad e_x = -v\sigma_z /E \tag{2.12}$$

$$e_x = \sigma_x / E \tag{2.13}$$

The general statement of Hooke's law can be shown as

$$e_x = (1/E)[\sigma_x - v(\sigma_x + \sigma_z)] \tag{2.14}$$

Principal stresses are the normal stresses which occur when all the shear stresses vanish. It is always possible to find a set of axes (1, 2, 3) on a body which creates the principal stresses. Principal stresses, *σ_1, σ_2, σ_3* can be defined as the three roots of (2.15)

$$\sigma_p^3 - I_1\sigma_p^2 - I_2\sigma_p - I_3 = 0 \tag{2.15}$$

where

$$I_1 = \sigma_{xx} + \sigma_{yy} + \sigma_{zz} , \tag{2.16}$$

$$I_2 = \sigma_{yz}^2 + \sigma_{zx}^2 + \sigma_{xy}^2 - \sigma_{yy}\sigma_{zz} - \sigma_{zz}\sigma_{xx} - \sigma_{xx}\sigma_{yy} , \tag{2.17}$$

$$I_3 = \sigma_{xx}\sigma_{yy}\sigma_{zz} + 2\sigma_{yz}\sigma_{zx}\sigma_{xy} - \sigma_{xx}\sigma_{yz}^2 - \sigma_{yy}\sigma_{zx}^2 - \sigma_{zz}\sigma_{xy}^2 \tag{2.18}$$

By using principal stresses, von-Mises stress can be calculated which is widely used in design as yielding criterion. Found von-Mises stress should be under the yield stress of the material, where the material starts to show plastic deformation. It basically takes into account all the principal stresses, σ_1, σ_2, σ_3 and expressed as

$$\sigma_v = \left[\frac{(\sigma_1 - \sigma_2)^2 + (\sigma_2 - \sigma_3)^2 + (\sigma_3 - \sigma_1)^2}{2} \right]^{\frac{1}{2}} \tag{2.19}$$

2.3 Fatigue Failure on Components

In most practical cases, the loading on the components fluctuates, generally in a random manner. Under the conditions of cyclic stress, generally found that the components fail much lower level of stress than would be expected where steady stress applied. This phenomenon is called fatigue and generally causes the majority of in-service fails.

Fatigue is defined as *"The process of progressive localized permanent structural damage occurring in a material subjected to conditions that produce fluctuating stresses and strains at some point or points and that may culminate in cracks or complete fracture after a sufficient number of fluctuations."* in ASTM standard E 1823 [3]. The necessity of three basic factors are stated for fatigue as "*a maximum tensile stress of sufficiently high value, a large enough fluctuation in the applied stress, and a sufficiently large number of cycles of the applied stress.*" [7]

The process of fatigue is usually divided into three regions:

- Crack initiation (nucleation, primary stage)

- Crack propagation (striations, secondary stage)

- Unstable crack propagation (tertiary stage)

Mainly, material type, load history, component processing and design effects the number of cycles require to fail. Most fatigue data are presented in the shape of S-N curves, which are the plots for cyclic stresses with respect to number of cycles to failure. The higher stress means the fatigue life drops progressively. In most applications, it is desired to use the component for a large number of cycles.

2.3.1 Defining Stress Cycles

There are many types of cyclic stress. Most commons are, *fully reversed cycle*, mostly used in testing, max and min stresses are equal but sign convention is different, no mean stress is available, *repeated stress cycle*, in which there is a mean stress, σ_m , additional to max and min stresses, *irregular (random) cycle,* in which the component is subjected to random loading during service. In this study, applied equivalent load from the mission is repeated stress cycle in which min stress is equal to zero.

Schematic of a cyclic stress is shown in Fig 2.1. Even it is generally drawn with sinusoidal waves; the actual wave shape has almost no importance. Another thing that frequency of the wave is also unimportant if it is small enough to give the component a break to dissipate the heat on. A basic term of a constant amplitude fatigue cycle is given below.
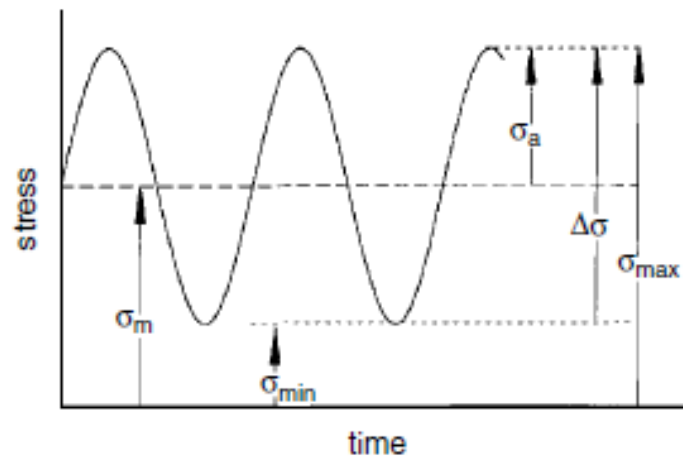
Fig 2.1 Schematic of cyclic stresses

The mean stress, σ_m , is defined as

$$\sigma_m = (\sigma_{max} + \sigma_{min}) / 2 \tag{2.20}$$

The amplitude, σ_a , is

$$\sigma_a = (\sigma_{max} - \sigma_{min}) / 2 \tag{2.21}$$

and the range, $\Delta\sigma$, is

$$\Delta\sigma = (\sigma_{max} - \sigma_{min}) = 2\sigma_a \tag{2.22}$$

Another used expression is the Ratio, R and defined as

$$R = \sigma_{min}/\sigma_{max} = (\sigma_m - \Delta\sigma/2)/(\sigma_m + \Delta\sigma/2) \qquad (2.23)$$

and amplitude ratio, A is defined as

$$A = \frac{\sigma_a}{\sigma_m} = \frac{1-R}{1+R} \qquad (2.24)$$

In this study, the ratio R is equal to zero and the ratio A is equal to 1, since the loading is defined as tension release.

2.3.2 S-N Curves

In the middle of 19th century, August Wohler performed the first systematic laboratory experiments to find out the reason why the repeated loading has high damage. [3] He tried to define the stress level below which the component will have indefinite number of cycles of life, defined today as *endurance limit* and also demonstrated that the applied stress range was more important than stress magnitude. Unlike Wohler test has limitations, today, to define an S-N curve based on test data, it is preferred to use a cylinder loaded in axial tension, free of sudden changes of the geometry and also with a polished surface on the critical section. Load is kept constant during the test. Further nominal stress, S, is calculated basically, and the results are plotted on a diagram. On x-axis, N is always plotted in logarithmic scale, while S is plotted on y-axis which might be linear or preferably logarithmic. An example of S-N curves is given in Fig 2.2. Mat A shows a typical curve for low carbon steel and other materials that strain-age. These type of materials have fatigue or endurance limits. The knee generally occurs around 10^6 cycles, although many materials such as aluminum alloys have no fatigue limit.
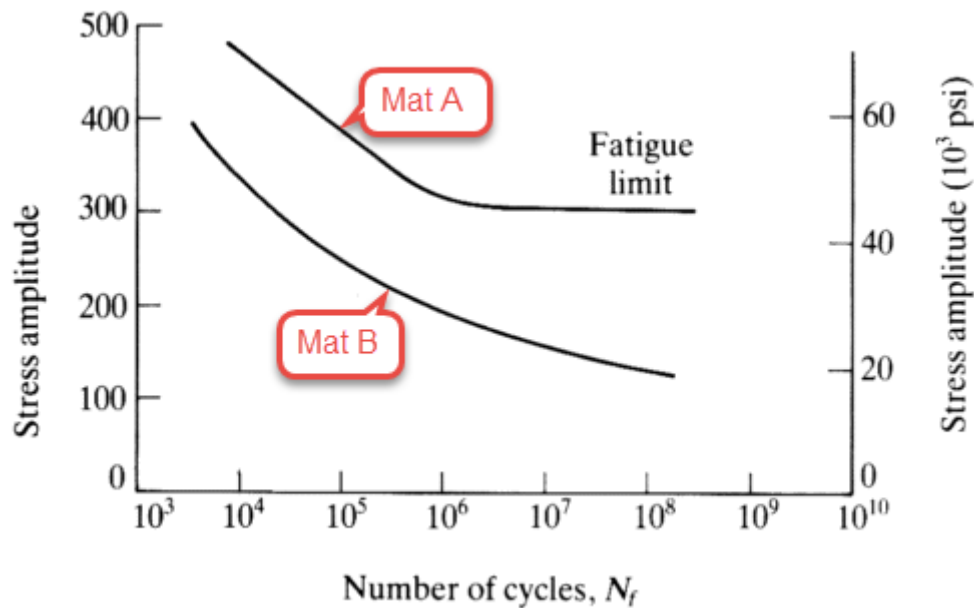
Fig 2.2 S-N curve example

2.3.3 LCF vs HCF

Low Cycle Fatigue (LCF) is usually considered to lead to failure in less than 10^5 cycles and High Cycle Fatigue (HCF) to lead to failure after more than 10^7 cycles. Also, transition point from LCF to HCF is generally assumed to occur where both elastic and plastic strains contribute to total strain equally. However, instead of number of cycles, the amount of damage accumulated during each load application is more important. For critical gas turbine components, LCF and HCF are generally separated from each other by defining the source of the loading; for LCF, the loading is caused mostly by pilot demands and the application of relatively large loads, while HCF is mainly driven by sources of vibration and the application of relatively small loads. [2]

Due to having high amplitude of cyclic stresses in LCF, the accumulated strain energy per reversal is significantly higher than HCF loading cycle; which leads to a behavior that life spent in crack initiation is small and the life spent in crack propagation is the significant proportion.

Most of the critical components of a gas turbine engine are subjected to very high loading cycles and therefore they are LCF life limited parts like the front bearing structure (FBS), the component used for this study.

2.4 Life Prediction Methods

Total life is determined by summation of crack initiation phase and crack propagation phase and the phases which each contribute vary with the loading, the geometry and especially with the material. As an example, ductile materials have more life in propagation phase while brittle materials have it for initiation phase. Two main life prediction methods used in FEA are strain-life and stress-life models.

Stress life is generally used for total life calculation. It is based on empirical S-N curves and then modified by a variety of factors generally coming from geometry. Generally these factors are taken from graphs and tables of stress concentration factors, but insufficient for the real geometry. FEA helps for these factors to be assumed and the material data is reduced and plotted as life N against nominal stress S. Comparing the stress data at the chosen critical point with this curve gives life estimation for the part. [8]

The S-N method is applicable to cases where all stresses remain elastic even the location where a crack will start and in application to FE models, linear elastic stresses from the analysis can be used directly to calculate the fatigue damage. Even it is more applicable to low load - long life problems, lives more than 10^4 cycles (HCF), designers use this methodology often.

Strain life methodology is adopted to use the strain response and to account for plasticity in the structure for such LCF problems. To start a crack, the strain should be plastic at some point. Fatigue is caused by strain and the properties of the material are changed by plastic strain, this is why cyclic material properties should be used.

It is based on the Strain Life Relation Equation shown in (2.25) where the parameters are specifically determined the best fit the equation to measured test data which will be terminated at the moment of the initiation of the crack. A total of six parameters should be defined, four strain-life parameter properties and two cyclic stress-strain parameters which are part of (2.26).

$$\frac{\Delta\varepsilon}{2} = \frac{\sigma_f}{E}\left(2N_f\right)^b + \varepsilon_f\left(2N_f\right)^c \qquad (2.25)$$

$$\Delta\varepsilon = \frac{\Delta\sigma}{E} + 2\left[\frac{\Delta\sigma}{K}\right]^{\frac{1}{n}} \qquad (2.26)$$

For both life prediction methods, some corrections are proposed to be accounted for the mean stress effect. Because, the cyclic fatigue properties are extracted from completely reversed loading in constant amplitude tests. In practical, this type of loading is not common. There is generally some mean stress and should be accounted. As well for stress-life method several empirical options exist like Gerber, Goodman and Soderberg, strain-life methodology generally uses Morrow or SWT correction. The Morrow mean stress correction method is briefly explained as below.

Morrow proposed that the mean stress could be accounted by modifying the elastic part of the Strain-Life curve by mean stress.

$$\varepsilon_a = \frac{(\sigma_f' - \sigma_0)}{E}\left(2N_f\right)^b + \varepsilon_f'\left(2N_f\right)^c \qquad (2.27)$$

Morrow correction is consistent with the observed values as mean stress effects are important for low plastic strain values while they have little effect at high plastic strains.

The strain life approach was more applicable than S-N method, which is found to be a subset of strain life method. This is assumed at long lives and elastic stresses, the two methods tend to be effectively the same. [8]

In this study, since the failure mechanism is LCF, strain-life methodology is preferred. But defining the strain life parameters was not easy for the component`s material, Ti 6-4. But in literature, a different approach is found which defines the parameters with respect to Brinell hardness of the material. For the fatigue analysis, strain-life parameters are taken from the study [9]

2.5   Fatigue Crack Initiation and Growth

The origin of most failures is pre-existing defects and flaws, such as cracks accidentally introduced into the structure. In many cases, the flaws had triggered fracture. But further, cracks can be initiated on the free surface of a part due to fatigue also. Different crack growth cases are given in Fig 2.3.
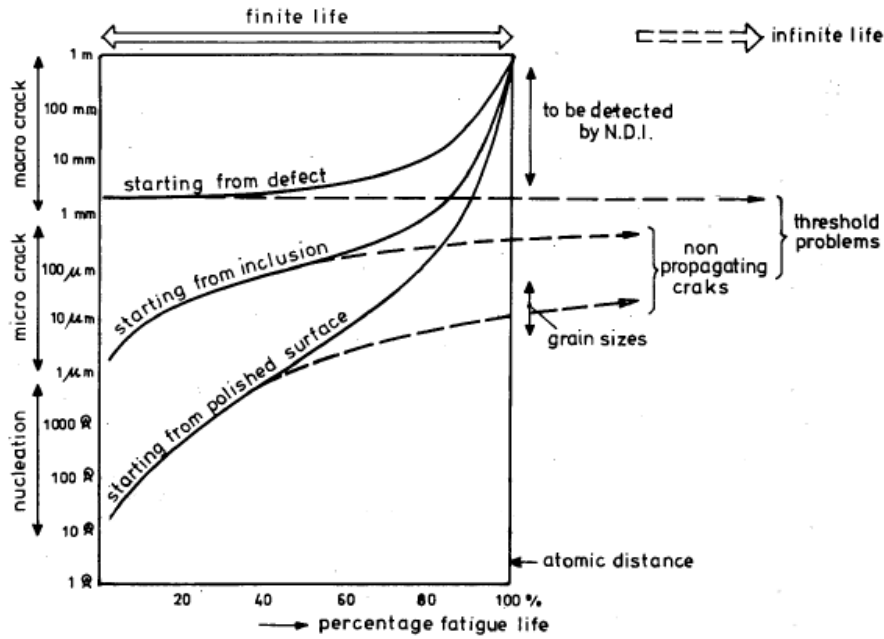
Fig 2.3 Survey of different crack growth cases [10]

Modes of fracture are introduced at this point. Irwin proposed a classification of three situations represented in Fig 2.4 which might enable a crack to propagate.
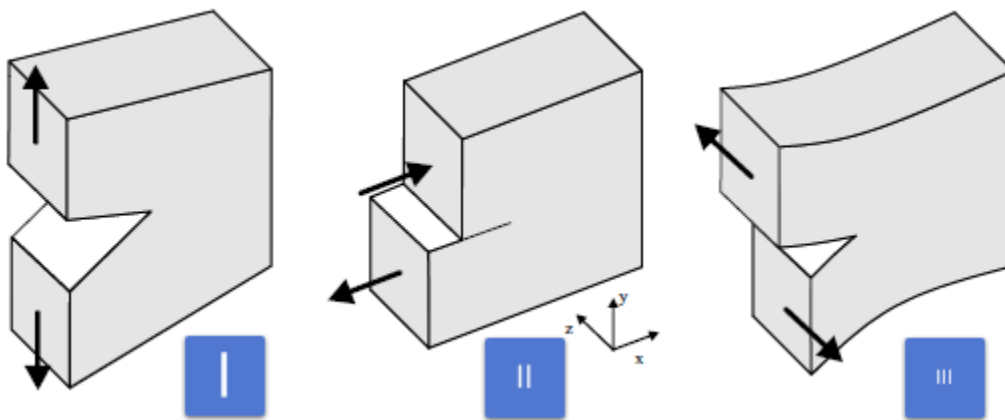

Fig 2.4 Crack modes [11]

In *mode I (opening mode)*, body is loaded by tensile forces, like the crack surfaces are pulled apart in y-axis. In the *mode II (sliding mode)*, the shear forces parallel to the crack surfaces is on the body and cause sliding over each other in x-axis, while in *mode III* which is *tearing mode*, the body is loaded by again with shear loads but this time parallel to the crack front of the crack surfaces causing sliding over each other in z direction. In practical, generally the crack propagation is observed as a superposition of these modes named as *mixed-mode*. [11]

As mentioned earlier, fatigue crack nucleation and growth occurs in three stages. It is marked on crack length - number of cycles (a-N) graph in Fig 2.5.
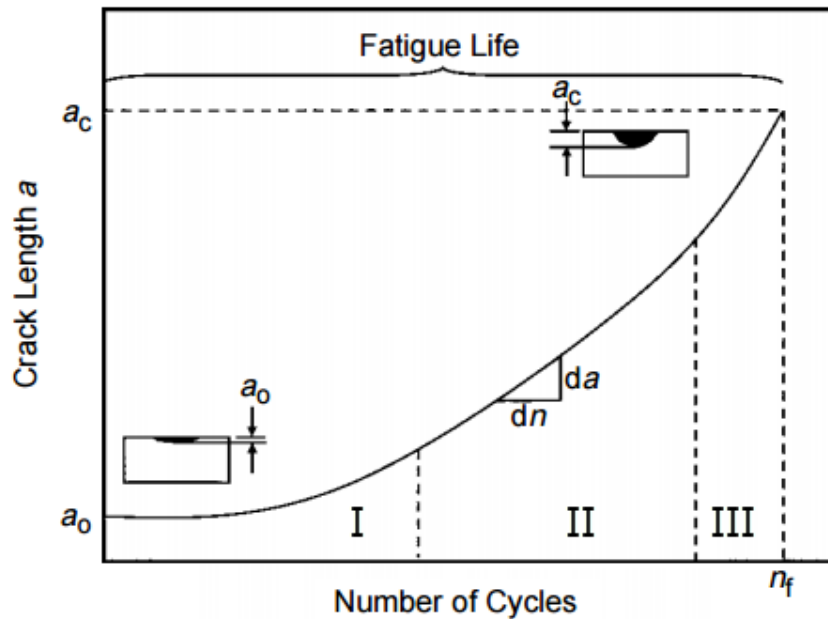
Fig 2.5 Crack length as a function of cycles [7]

Stage-1, (nucleation) is stated "*Crack initiation usually starts at a notch or other surface discontinuity. Even in the absence of a surface defect, crack initiation will eventually occur due to the formation of persistent slip bands.*" [7] In this stage, the fatigue crack tends to propagate initially along slip planes and later takes the direction normal to the maximum tensile stress. The crack propagation rate is very low during stage-1, nearly 1 nm per cycle and it spends 90% of the fatigue life. The crack enters stage-2, when the overall crack plane changes and becomes perpendicular to the principal stress at the point the crack length becomes sufficient for the stress field at the tip to become dominant. [7]

In *stage-2*, crack propagates in a direction to normal to the applied stress. It grows by a continual process of crack sharpening followed by blunting. This produces a pattern of fatigue striation with each striation represents one cycle of fatigue. These striations prove that stress changes during fatigue. [12]

Stage-3 is the region when unstable fatigue crack propagation leading to failure is observed. The reason stated as "*Ultimate failure occurs when the fatigue crack becomes long enough that the remaining cross section can no longer support the applied load.*" [7]

17

2.5.1 Fatigue Constant Amplitude Crack Propagation

Linear elastic fracture mechanics assumes that every structure has flaws. Crack grows from initial size a0 to critical size ac as a function of number of load cycles. Crack growth rate is initially slow, and then the rate goes up as the crack grows. The slope of the curve gives the growth rate. (Fig 2.5) It depends on the length of the crack and the stress range, $\Delta\sigma$.

The stress intensity factor, K on the crack tip is preferred as a parameter to control the crack propagation rate by Paris and Erdogan. They tested high strength aluminum panels with a crack on centre. The experimental results showed that the crack growth rate acted with parallel to crack length changing with stress intensity factor. It is concluded that

$$\frac{da}{dN} = f(\Delta K)$$

(2.28)

where $\Delta K = K_{max} - K_{min}$, using the σ_{max} and σ_{min} respectively. [12]

In region-II, crack growth rate is stable and essentially linear and it is modeled with a power equation to fit the experimental data by Paris and Erdogan as follows,

$$\frac{da}{dN} = C(\Delta K)^m$$

(2.29)

In Paris equation, *a* is the crack size; *n* is the number of cycles. Constant parameters C and m depends on the material variables, environment, temperature and fatigue stress conditions. [7] These parameters should be determined experimentally. For metals, m is in the range of 2-4.

If three regions of crack propagation is associated with ΔK;

The low end of ΔK is in Region-1 where the growth rate rapidly decreases with decreasing ΔK and reaches out to K_{th} which the threshold value to a crack. Under this value no crack are observed. In Region-2, crack growth is stable and the rate depends on the power law. Rapid crack growth is seen in Region-3 near the high end of ΔK curve while K_{max} approaches to K_c. In this region, local static modes of fracture start to dominate the behavior.

In the Region-2 where crack growth is linear, number of cycles to failure can be determined from the Paris law as

$$dn = \frac{da}{C(\Delta K)^m} \tag{2.30}$$

The integration gives

$$n_f = \int_0^{n_f} dn = \int_{a_0}^{a_c} \frac{da}{C(\Delta K)^m} \tag{2.31}$$

ΔK can be expressed in terms of Δσ:

$$\Delta K = Y \, \Delta\sigma \, \sqrt{\pi a} \tag{2.32}$$

where Y depends on the specific specimen geometry, if Δσ is assumed to be constant and Y to be dependent to crack length. So if (2.32) is replaced into (2.31)

$$n_f = \frac{1}{C\pi^{m/2} (\Delta\sigma)^m} \int_{a_0}^{a_c} \frac{da}{Y^m a^{m/2}} \tag{2.33}$$

which gives the number of cycles to failure. Solving this equation requires using numerical iterations in case the Y depends on the crack length. In Region-2, some metal crack growth behavior is affected by R-ratio. It is stated as effect of mean load. Paris law does not account this effect.

Further, Foreman and his associates developed (2.34) to take into account the effect of R-ratio.

$$\frac{da}{dn} = \frac{C(\Delta K)^m}{(1-R)K_c - \Delta K} \tag{2.34}$$

A typical fatigue crack propagation behavior and logarithmic crack growth curves for different R-ratios is given in Fig 2.6.
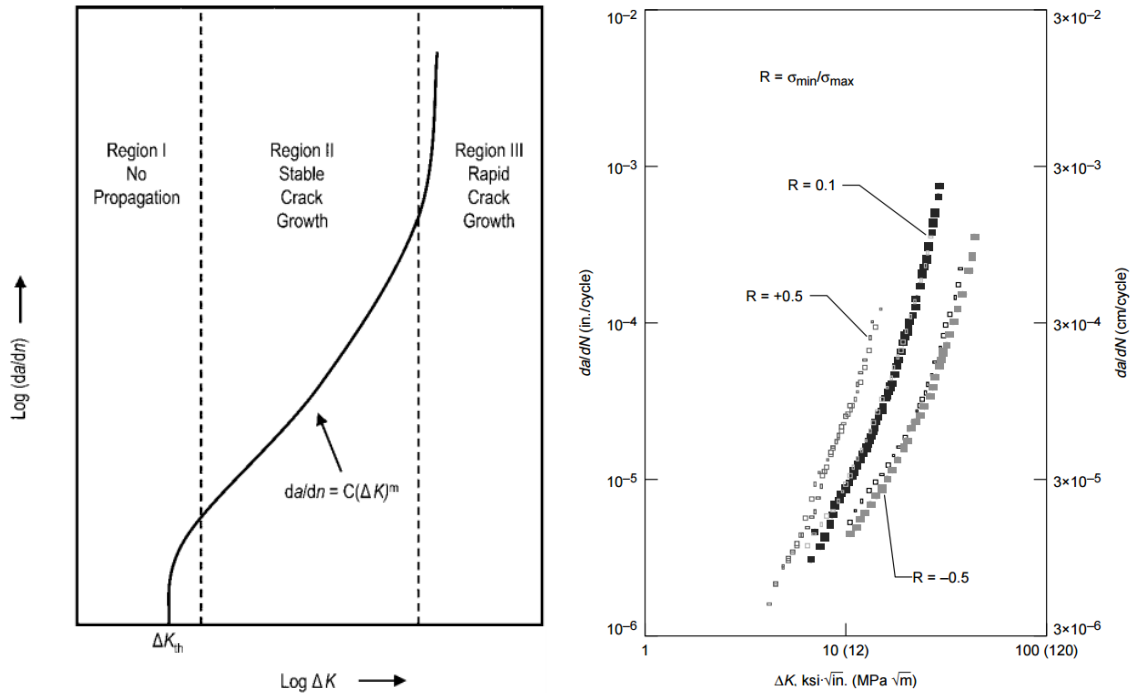
Fig 2.6 Crack propagation curves for fatigue loading [7]

2.6 The J-integral Fracture Criteria

In this study, J-integral concept is used to predict the behavior of the crack defined on the FBS. The J-integral is one of two concepts related to elastic-plastic fracture mechanics (EPFM). Other one is crack opening displacement.[14]

J-integral is a path independent line integral which is the two dimensional version of the conservation law introduced by Rice for notch problems. Its use for plasticity type materials has been supported by experimentation or numerical analysis, though J-integral is based on purely elastic analysis.

2.6.1 Path Independent Integrals

It is assumed a solid body which is elastic, homogeneous, anisotropic and under a static equilibrium with a traction Tk. A bounding surface denoted by Σ of the region R occupied by the body is defined and all quantities to a fixed Cartesian coordinate system $Ox_1x_2x_3$. The deformation is assumed small. Based on all these assumptions, the stress tensor σ_{ij} is obtained from the elastic strain energy ω as

$$\sigma_{ij} = a_{ij} = \frac{\partial w}{\partial \varepsilon_{ij}}, w(0) = 0 \tag{2.35}$$

The strain tensor denoted with ε_{ij}. The strain energy density is considered to be continuously differentiable with respect to strain. For elastic behavior, it becomes (2.36), where the integral is path independent in the strain space.

20

$$w = \int_0^{\varepsilon_{kl}} \sigma_{ij} d\varepsilon_{ij} \tag{2.36}$$

If the body forces are zero, the equations of equilibrium and the traction vector T_j on surface S are given in (2.37) and (2.38).

$$\sigma_{ij,i} = \frac{\partial \sigma_{ij}}{\partial x_i} = 0 \tag{2.37}$$

$$T_j = \sigma_{ij} n_i \tag{2.38}$$

where n_i denotes the normal vector. The strain tensor is derived from the displacement field as shown for small deformation.

$$\varepsilon_{ij} = \varepsilon_{ji} = \frac{1}{2} (u_{i,j} + u_{j,i}) \tag{2.39}$$

The integrals are reminded where a closed surface Σ bounding a region R which is assumed to be free of singularities.

$$Q_j = \int_\Sigma (w n_j - T_k u_{k,j}) \, d\Sigma \ , j, k = 1,2,3 \tag{2.40}$$

After Gauss` divergence theorem

$$Q_j = \int_R (w \delta_{jl} - \sigma_{lk} u_{k,j}) \, , l \, dV \tag{2.41}$$

Working the equation out with (2.35) and (2.36) gives

$$(w \delta_{jl} - \sigma_{lk} u_{k,j}), l = -\sigma_{kl} r_{kl,j} = 0 \tag{2.42}$$

r_{kl} denotes the non-symmetrical rotation tensor for small deformation given by

$$r_{ij} = -r_{ji} = \frac{1}{2} (u_{i,j} - u_{j,i}) \tag{2.43}$$

In the end,

$$Q_j = 0 \tag{2.44}$$

2.6.2 Definition of J-integral

For the particular case of the two-dimensional plane elastic problem, the integral is given in (2.45)

$$J = Q_1 = \int_\Gamma (wn_l - T_k u_k \,_{,1})ds \tag{2.45}$$

where Γ is a closed contour bounding a region R shown in Fig 2.7.
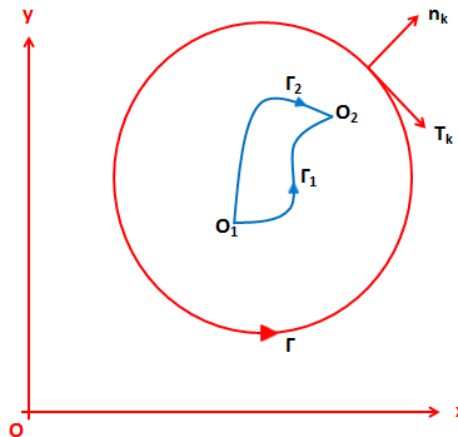
Fig 2.7 A closed contour and paths between two points

With $n_1 = (dy/ds)$, (2.45) becomes

$$J = \int_\Gamma wd_y - T_k \frac{\partial u_k}{\partial x} \, ds \ (k = 1,2) \tag{2.46}$$

It defines the J-integral along a closed contour in two-dimensional space. It is already known that $Q_j=0$ from (2.44), it follows that $J=0$. Since J is zero for any closed paths, the J-integrals along any two paths Γ_1, Γ_2 connecting any two points O_1, O_2, are equal. Finally,

$$J_1 = J_{\Gamma_1}[...] = J_2 = \int_{\Gamma_2}[...] \tag{2.47}$$

2.6.3 Application to notches and cracks

It is assumed a crack that has parallel flat surfaces to x-axis which have a random root radius as shown.
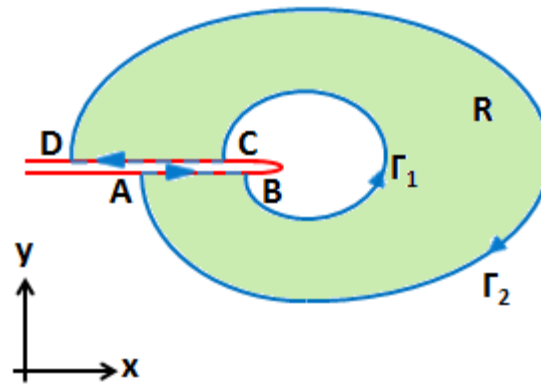
Fig 2.8 Paths around a crack tip

The region R bounded by the closed contour AB Γ_1CDΓ_2A is free of singularities and the J-integral calculated along this closed path is zero.

$$J_{AB\Gamma_1CD\Gamma_2A} = J_{B\Gamma_1C} + J_{CD} + J_{D\Gamma_2A} + J_{AB} = 0 \qquad (2.48)$$

AB and CD of the crack surfaces are parallel to the x-axis and they are traction free. So, dy=0 and T_k=0. (2.48) becomes

$$J_{B\Gamma_1C} = J_{A\Gamma_2D} \qquad (2.49)$$

which proves the path independence of the J-integral for crack problems. It gives the flexibility to choose the integration path far away from the crack tip to make the calculation easier under the circumstances that crack surfaces are parallel to x-axis and traction free.

2.6.4 Relationship between the J-integral and Potential Energy

In this part, a physical interpretation of the J-integral in terms of the rate of the change of potential energy with respect to incremental change of crack size is tried to derive.[14] In the beginning following assumptions are made:

- A linear or nonlinear elastic plane body with a crack of length a is subjected to defined tractions and displacements along parts of its boundary (Fig 2.9).

23
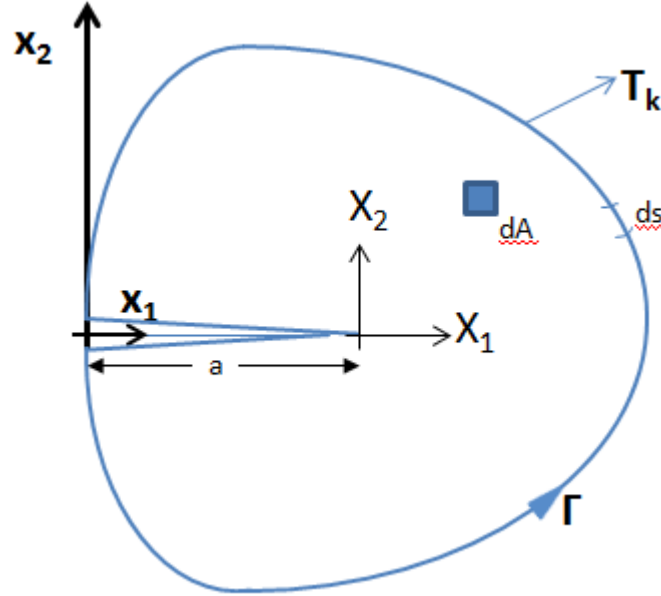
Fig 2.9 A two-dimensional cracked body

- The tractions and displacements are independent of crack length.

- The body is attached to a fixed system of Cartesian coordinates x_1x_2 and the crack surfaces are parallel to x-axis.

- The crack extends in a self-similar manner.

The potential energy $\Pi(a)$ of the body is given by

$$\Pi(a) = \int_A w \, dA - \int_\Gamma T_k u_k \, ds \tag{2.50}$$

where A is the area of the body and Γ is the boundary. If the (2.50) is differentiated with respect to crack length a and a new coordinate system X_1X_2 is attached to the crack tip, the equations takes the form

$$\frac{d\Pi}{da} = \int_A \left(\frac{\partial w}{\partial a} - \frac{\partial w}{\partial x_1}\right) dA - \int_\Gamma T_k \left(\frac{\partial u_k}{\partial a} - \frac{\partial u_k}{\partial x_1}\right) ds \tag{2.51}$$

(2.31) is recalled and the principle of virtual work is applied, (2.52) is found as follows.

$$\frac{d\Pi}{da} = \int_A \left(\frac{\partial w}{\partial a} - \frac{\partial w}{\partial x_1}\right) dA - \int_\Gamma T_k \left(\frac{\partial u_k}{\partial a} - \frac{\partial u_k}{\partial x_1}\right) ds \tag{2.52}$$

Furthermore, the divergence theorem yields

$$\int_A \frac{\partial w}{\partial x_1} \, dA = \int_\Gamma w dx_2 \tag{2.53}$$

(2.52) and (2.53) are introduced into (2.51). For any path of integration surrounding the crack tip, J-integral is found by

$$-\frac{d\Pi}{da} = \int_\Gamma w \, dx_2 - T_k \frac{\partial u_k}{\partial x_1} \, ds \tag{2.54}$$

$$J = -\frac{d\Pi}{da} \tag{2.55}$$

This shows that the J-integral is the rate of decrease of potential energy with respect to the crack length if only self-similar crack growth is assumed.

2.6.5 Relationship between J-integral and Fracture Toughness

Fracture toughness, K_{Ic} is a material property which describes the resistance capacity against fracture. Also, plastic-elastic fracture toughness is denoted by J_{Ic}. For isotropic, linear elastic materials, if the crack is growing straight ahead with respect to its original location, the relation between K_{Ic} and J_{Ic} is as

$$J_{Ic} = K_{Ic}^2 \left(\frac{1 - v^2}{E}\right) \tag{2.56}$$

2.6.6 J-integral Fracture Criterion

The J-integral is accepted as a parameter which characterizes the terms of the region around the crack tip. The following fundamental properties of J supports that [13]:

- For linear/nonlinear elastic material response, J is path independent and equal to - dΠ/d*a.*

- J is equal to G, the value of energy release rate.

- It can be determined experimentally.

- It can easily be related to the crack tip opening displacement, δ by *J=Mσ$_Y$δ* (For Dugdale model M=1)

J-integral is a catchy candidate for fracture criteria, because of the properties above. Under mode-I loading, the criterion of crack initiation is defined as follows

$$J = J_C \qquad\qquad (2.57)$$

where J_c is a material property under certain environmental conditions for a given thickness. The critical value of J, denotes as J_{lc}, is related to *fracture toughness* K_{lc}, all under plane strain conditions, by

$$J_{Ic} = \frac{1 - v^2}{E} K_{IC}^2 \qquad\qquad (2.58)$$

In this study, for the given part, the FBS, initial cracks are defined through the parametrical geometry on the solid body. Different sizes of cracks are modeled which all the crack surfaces are on the same plane and parallel. With the help of a finite element analysis program, J-integral values are gathered from the tips of the cracks and they are used to predict the behavior of the crack.

2.7 Finite Element Modeling

Finite Element Method, which is sometimes referred to Finite Element Analysis, is nothing but simplifying a problem by dividing it into small problems instead of solving a complex problem. This should be considered that, since the problem is replaced with other problems, solution will be an approximation. But for most of the practical problems, any existing mathematical tool will not be sufficient, so finite element method is needed. Also finite element method is open to improve or refine the results. It is basically based on the interconnected sub regions named as finite elements that are built in the real geometry and with a good enough approximation this will direct us to the results.

2.7.1 Brief History of FEM and Preferred Software

Even its mathematical history goes much earlier, finite element method had its real start in 1940s when Courant introduced the concept of piecewise-continuous functions in a sub domain. In the late 1940s, without any digital computation, the application of simple finite element method is seen in aircraft calculations, known as flexibility method. Afterwards, finite element method has found more application areas with an impressing rate, parallel to raise in the performance of computers. In 1960, the name finite element is first stated by Clough in the context of plane stress analysis. For the next two decades, 1960s and 1970s, finite element method has found extended application areas from structural to fluid flow, heat transfer. Przemieniecki's book presents the finite element method to solve the stress analysis

problems, while Zienkiewicz and Cheung presents the general explanation of the method and the applicability to any general field problem. This led to further with deriving the finite element equations by using weighted residual method, most known as Galerkin method. [14], [15]

Different commercial software codes are developed for calculation like Nastran, Ansys, Algor etc. and they allow us to use the finite element method for different, complex problems in our desktops with the limitation of computational environment.

In this thesis, ANSYS Classic which will be referred as Ansys in further recalls and ANSYS WB are preferred as FE modeling and solver tool. The previously validated FE model under unit loading test data, which will not find a place in this thesis due to propriety information of the company, was prepared with Ansys. Because of the experience and know-how built for years and the control capability on meshing, modeling and solvers, ANSYS Classic is considered as a platform which is more stable, reliable and restrained by user. Even so, due to convenience of modeling the crack and getting the results as fastest as possible, main tool is selected as Ansys WB and the primary results of principal stresses near the area of interest are checked with the results coming from the platform Ansys. Fatigue and crack propagation analyses are done by using Ansys WB, since the results from primary analysis is consistent with Ansys.

3   FINITE ELEMENT STUDY

In this Chapter, definition of the geometry, prepared FE model, in details, geometrical adjustments, meshing details and loading/boundary conditions are explained. The results of the static analyses for comparison between ANSYS Classic and Workbench have been stated. Further, the life is estimated by Strain-Life methodology. At the end, a crack is implemented in the model and the results of K_I and J-integral through different crack lengths are shared.

3.1   Definition of Front Bearing Structure (FBS)

The FBS is a radial structure being part of the main load path of the engine. It provides load path by a Central Tube (CT) at the Front Frame (FF) inner ring and two Engine Bars at port and starboard locations between the Propeller Gear Box (PGB) and the turbo machinery. Front engine configuration is shown below in Fig 3.1.
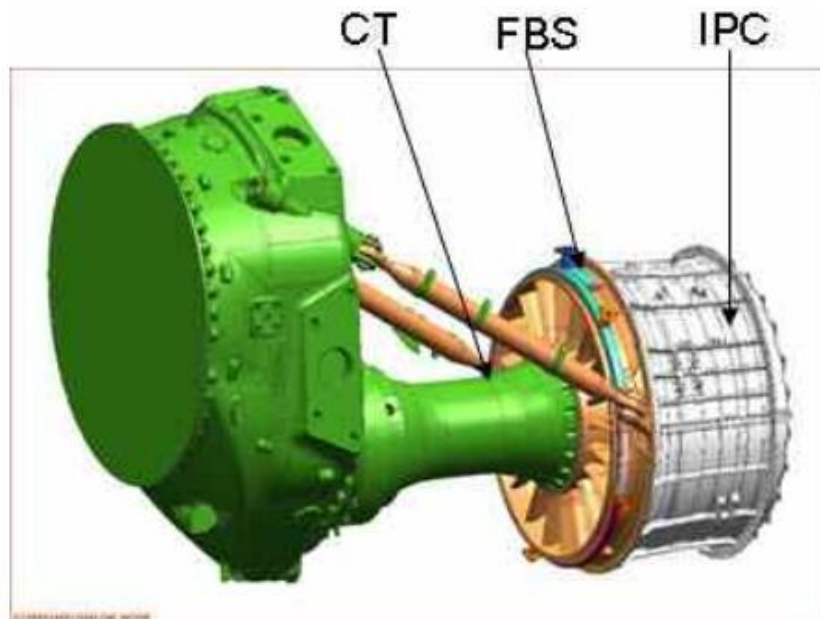
Fig 3.1 Front Engine configuration

The FBS is designed to support bearing loads coming from intermediate shaft and low pressure shaft thrust. Until the engine is ignited to become stable, it covers the torque produced, also it holds against the load coming from the engine bars. Another structural job, it is done by the FBS is carrying the axial load of the air taken into the compressor. Besides these structural duties, the FBS has aerodynamic role as correcting the deflection given to the air by the propeller and the intake duct before it enters into the first rotor stage of the Intermediate Pressure Compressor (IPC). Also it

is capable of anti-icing and management of the oil in the bearings on front and behind it.

The FBS has two main parts; front frame and rear bearing support. The front frame is designed to be aerodynamically appropriate and has 20 Inlet Guide Vanes (IGV) which are all different to each other, Fig 3.2.
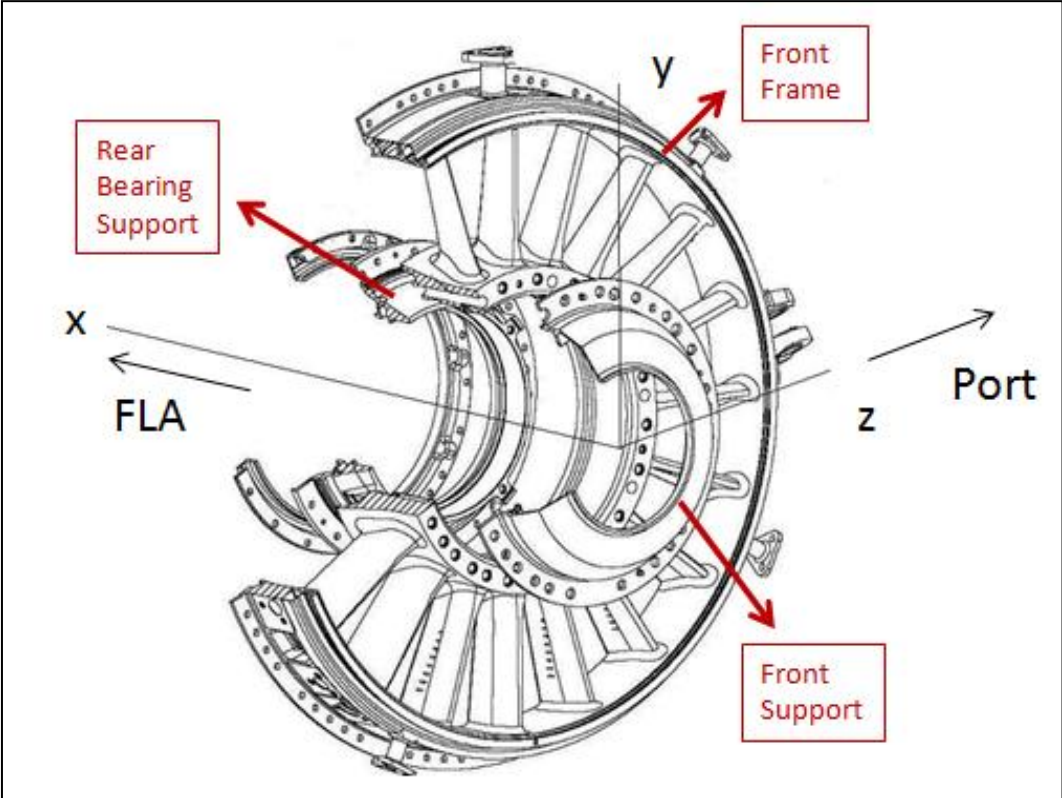
Fig 3.2 Geometry of the FBS

Average outer diameter of the front frame is 70 centimeters, while the vanes are 15 centimeters long radially. Twenty vanes are placed in every 18 degrees tangentially. The angle between the two lugs which are on port and starboard directions to carry loads coming from engine bars is nearly 165 degrees, equally placed on top half with respect to engine axis - x forward looking aft.
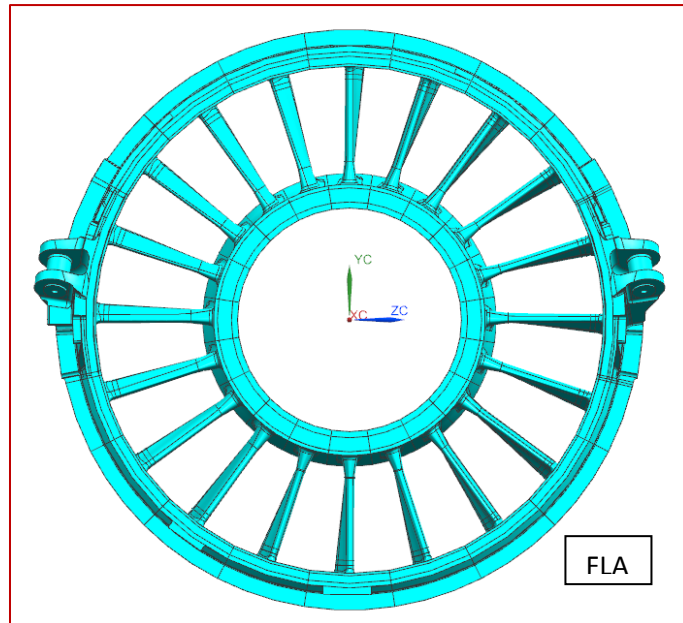
Fig 3.3 Vane Structure forward looking aft

3.2 Material Properties

The FBS is made of Ti-6V-4Al as known in market Ti 6-4. The raw material is manufactured by casting or forging for different trials.

In this thesis, the one used is produced by casting. Main elastic properties are given in Table 3.1 below.

Table 3.1 Elastic properties of Ti-6Al-4V

Identification	Description	Value
E	Elastic Modulus (GPa)	115
v	Poisson's Ratio	0.31
Sy	Yield Strength (MPa)	786
UTS	Ultimate Tensile Strength (MPa)	862

3.3 Preparation of Static FE Model in ANSYS Classic and ANSYS WB

Front Frame and Rear Bearing Support are used in test rig as real manufactured parts. Intermediate Pressure Compressor (IPC) casing and Central Tube (CT) are manufactured as dummy and disposable components. All components that are modeled with Ansys have same geometrical description as in test rig. Except front frame and rear bearing support, other parts are modeled to cover the real parts strength. Some bolt holes, radiuses and unrelated features are not modeled, assumed that they do not affect the results in the area of interest.

3.3.1 Preparation of CAD Model

Front Bearing Structure contains very complex geometrical features because of having a duty like controlling oil management. So, it is not so easy to model in FE modeling programs. Hence, the explained procedure is followed:

- The whole test rig specimen and adjacent parts are modeled in the CAD program with defined dimensions with every little feature on it.
- Little features like chamfers or blends located far enough to area of interest which will not be affect model's stiffness are deleted. Model is cleaned up in tolerance 0.01 micron.
- It is split into more little parts to build a model with using as much as brick elements that will be explained in next section. Giving enough space to transition elements is considered during this process.
- Parts that are same, can be meshed by copying, reduced into only part.

For Ansys and Ansys WB, different splitting strategies are developed. The number of parts before modeling in Ansys is much more than the number of parts will be modeled in Ansys WB. The reason for this is the meshing in Ansys is more challenging. On every area which is shared by different volumes, mesh should be compatible to get results without having contact elements. Here is where the *mesh dependent* concept is introduced.

For Ansys WB, definition of mesh is different. Unlike Ansys, all geometrical features are stored in FE model in Ansys WB, in the meaning of elements and nodes are kept attached to solid geometry to have the flexibility of applying loads on geometry. At some locations, independent mesh is allowed and contact elements are used to have connections between elements on different convergent faces. Number of parts meshed in Ansys WB is limited not only to easily control the number of contacts, but also to keep the error coming from contact non-linearity in tolerances.

Different views of the chunked geometry which will be used for modeling in Ansys and Ansys WB are shown in Fig 3.4.

31
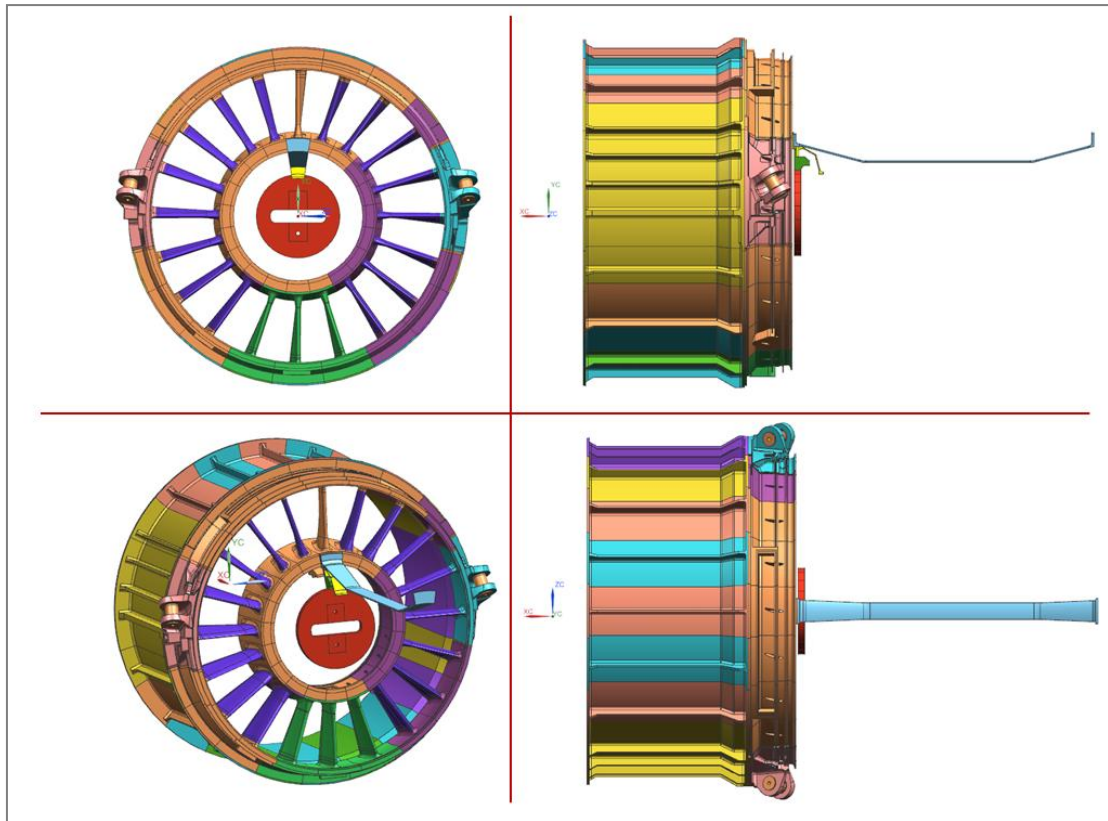
Fig 3.4 Chunked geometry of the FBS

Counted number of parts in comparison:

Table 3.2 Number of parts

Tool	# of Parts
Ansys	583
Ansys WB	47

3.3.2 Meshing Details

The components especially the front frame are wide, heavy parts. The diameter is nearly 70 centimeters. Because of that, modeling the components in ANSYS is not easy. If total node number is too much, it will cause some difficulties, like calculation time. Mesh size should be big enough to reduce the total element and node numbers, but small enough to reflect the real geometry and stiffness value. In order to achieve that, element size is not constant through the whole mesh. It is refined near the area of interest while it is kept coarser especially on adjacent parts.

3.3.2.1 Element Types

The use of tetrahedron elements in all components would cause the excessive raise in defined number of nodes. Hence, in FE model, brick (HEX) elements are used as

the geometry allows instead of tetrahedron (TET) elements. Wedge elements which are transition elements are also used. But still, instead of linear elements, second order elements which have tolerance to loss of accuracy are preferred which are named as SOLID95 (SOLID 186) and SOLID92 (SOLID187) because of having a lot of irregular shapes. These elements have compatible displacement shapes and they are good at modeling curved boundaries.

In general, these element types have three degree of freedom on each node as translation in nodal three directions (x, y and z). In Ansys, they are standing as elements which have different capabilities like plasticity, creep, stress stiffening, large deflection and large strain.

Besides solid elements MASS21 element type is also used in the model. Generally this element is used to model non-structural components, dead loads like dampening and damper rings if you enter a value as mass. In this case, the stiffness of the part is assumed negligible. But on the other hand, if the mass value is not entered to the model as a real constant, generally this element is used to create only an application point to loading.

3.3.2.1.1 Definition of SOLID186

SOLID186 is the type of solid element which has 20 node in 3D. It exhibits quadratic displacement behavior. Further description is stated in Ansys manual as "*The element is defined by 20 nodes having three degrees of freedom per node: translations in the nodal x, y, and z directions. The element supports plasticity, hyperelasticity, creep, stress stiffening, large deflection, and large strain capabilities. It also has mixed formulation capability for simulating deformations of nearly incompressible elastoplastic materials, and fully incompressible hyperelastic materials.*" [16]

SOLID186 have two forms available; homogenous structural solid which is like in these FE models and layered structural solid. Homogenous structural solid SOLID186 is good at modeling irregular meshes, like getting into shape tetrahedral, pyramid or prism. These shapes can be found by giving the same node number to some nodes as shown in Fig 3.5.
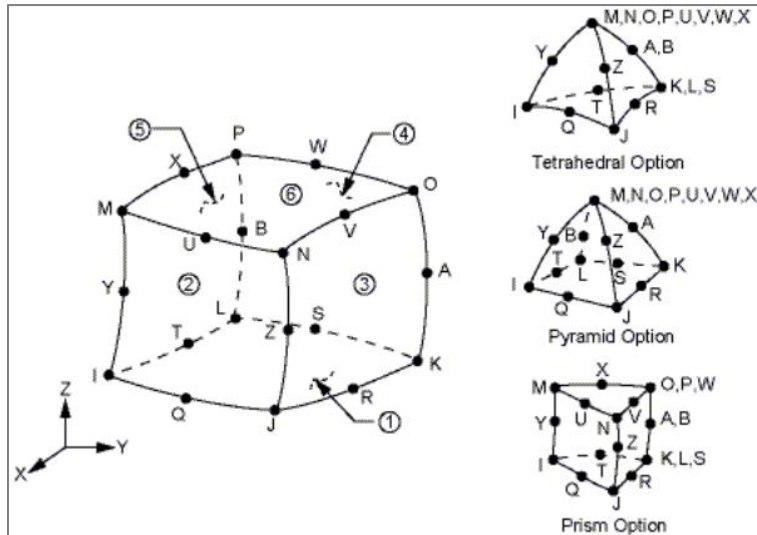
Fig 3.5 SOLID186 homogenous structural solid geometry

3.3.2.1.2 Definition of SOLID187

SOLID187 is 10-node, higher order 3D element. Like SOLID186, it has quadratic displacement behavior and well suited to irregular meshes. The description in Ansys manual is "*The element is defined by 10 nodes having three degrees of freedom at each node: translations in the nodal x, y, and z directions. The element has plasticity, hyperelasticity, creep, stress stiffening, large deflection, and large strain capabilities. It also has mixed formulation capability for simulating deformations of nearly incompressible elastoplastic materials, and fully incompressible hyperelastic materials.*" [16]

Shape of the element type is like the tetrahedral option of the SOLID186 element as shown in Fig 3.6. This element type is used to model complex geometries with TET elements.
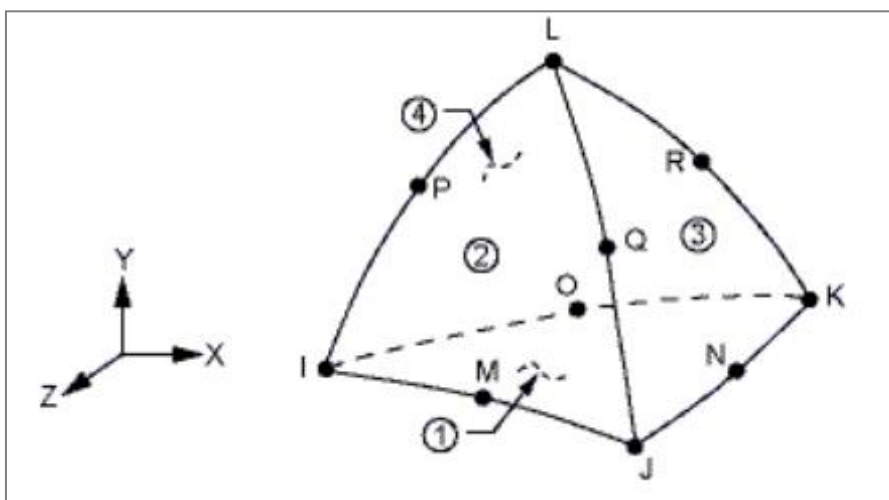
Fig 3.6 SOLID187 structural solid geometry

34

3.3.2.1.3 Definition of MASS21

Mass21 is type of element which is a structural mass. Degree of freedoms for this type of element can be defined up to six, which are translations in nodal x, y and z directions and rotations about the nodal x, y and z axes. It is a point element which is dimensionless. Hence, different masses and rotary inertias can be assigned to each coordinate direction. [16] The basic illustration of the element is like in Fig 3.7.

It has options like 3D/2D mass with or without rotary inertia. In this FE model, Mass21 is used without defining any mass value, just to apply loads from one point.
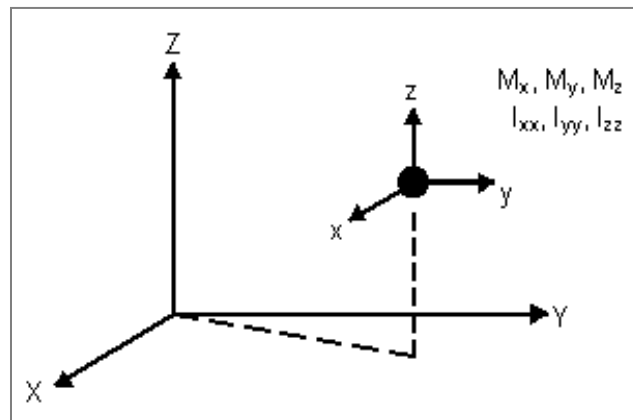
Fig 3.7 MASS21 point element

3.3.2.2 Meshing Details in ANSYS Classic

Structural solid elements are used to model the bodies. Element options are left as default. For Solid186 uniform reduced integration method is used as element technology. It provides help to prevent volumetric mesh locking in nearly incompressible cases. [16] For both Solid186 and Solid187, pure displacement element formulation is chosen, since no elastoplastic or hyper elastic materials are defined in the model. Solid bodies can be shown below, Fig 3.8.
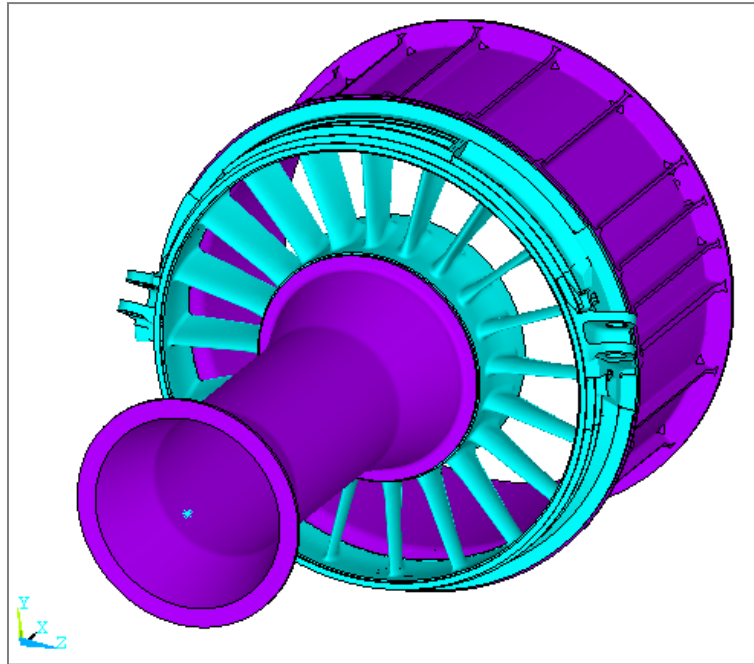
Fig 3.8 Solid bodies

Under the limitation of total node and element number, model mesh is optimized. Total node and element numbers Table 3.3 and plots Fig 3.9 related to FE model mesh can be found below.

Table 3.3 Numbers of elements and nodes

	#
Elements	1029443
Nodes	2099439
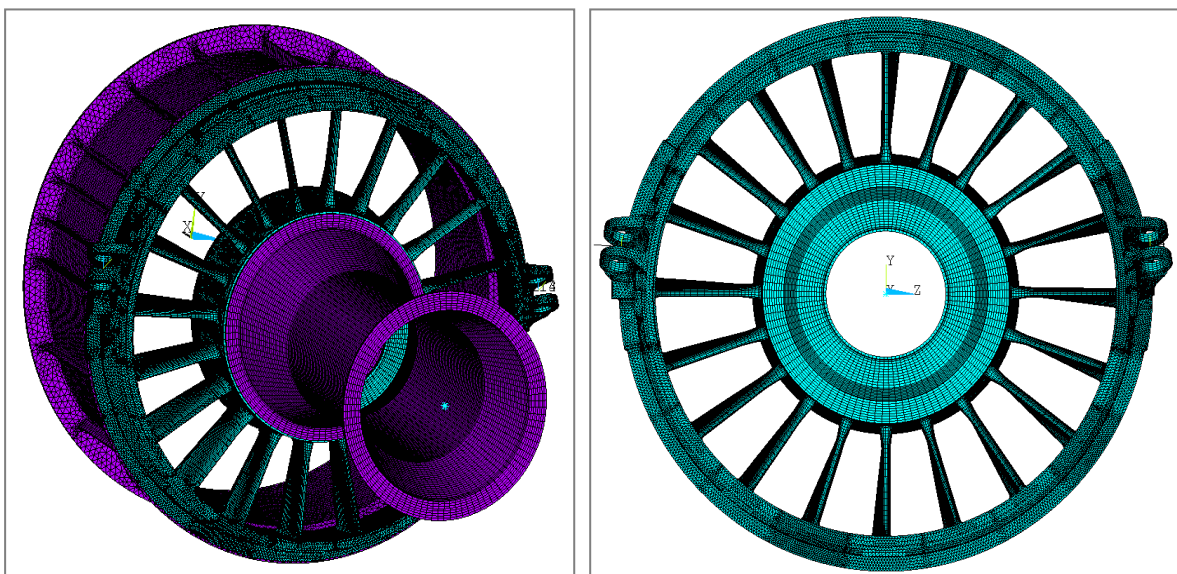
Fig 3.9 Mesh details of FBS

3.3.2.3 Meshing Details in ANSYS WB

On the contrary of Ansys, in Ansys WB, there is no need to prepare a model with a lot of solid volumes sharing the same areas. When the user import the geometry into the program, it directly identifies the areas that are in some tolerance to be contacted. When the geometry first imported these contact areas should be revised. If the model is clear, then meshing process starts.

Thanks to improvement in Ansys WB mesher tool, it is capable to prepare *hex dominant meshed* models, which still contain tetrahedral elements but if it is only necessary in complex geometries. It also gives chance to define element sizes or line sets which contributes the user control on meshing.

In this FE model, vane volumes are meshed with hex elements and other parts meshed as hex dominant. Also the locations that the crack initiation is expected meshed more carefully with finer elements. The number of defined elements and nodes is given in Table 3.4.

Table 3.4 Number of elements and nodes

	#
Elements	714059
Nodes	1850652

General view of prepared mesh and detailed plots can be found in Fig 3.10-11.
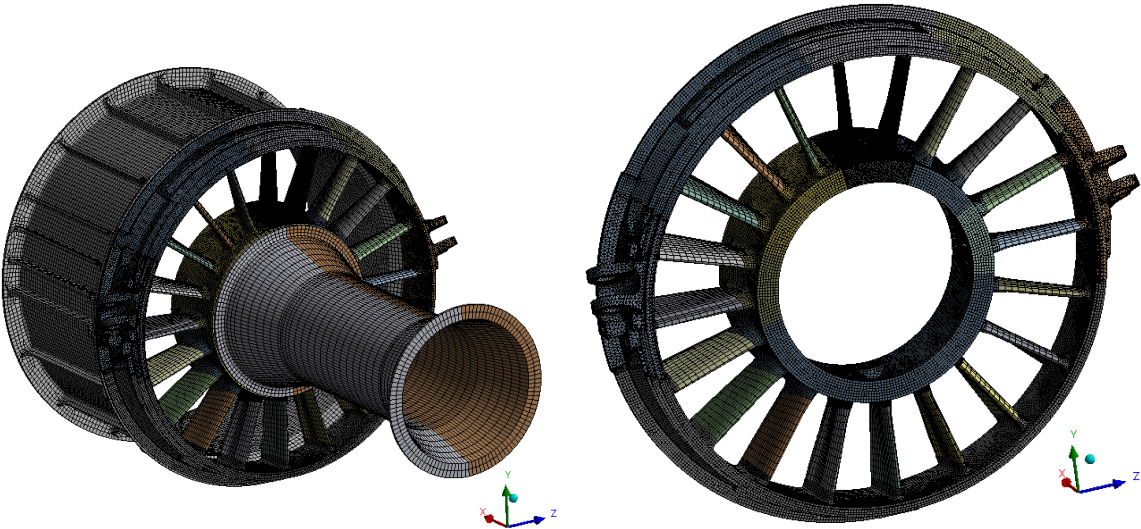
Fig 3.10 Mesh details in Ansys WB
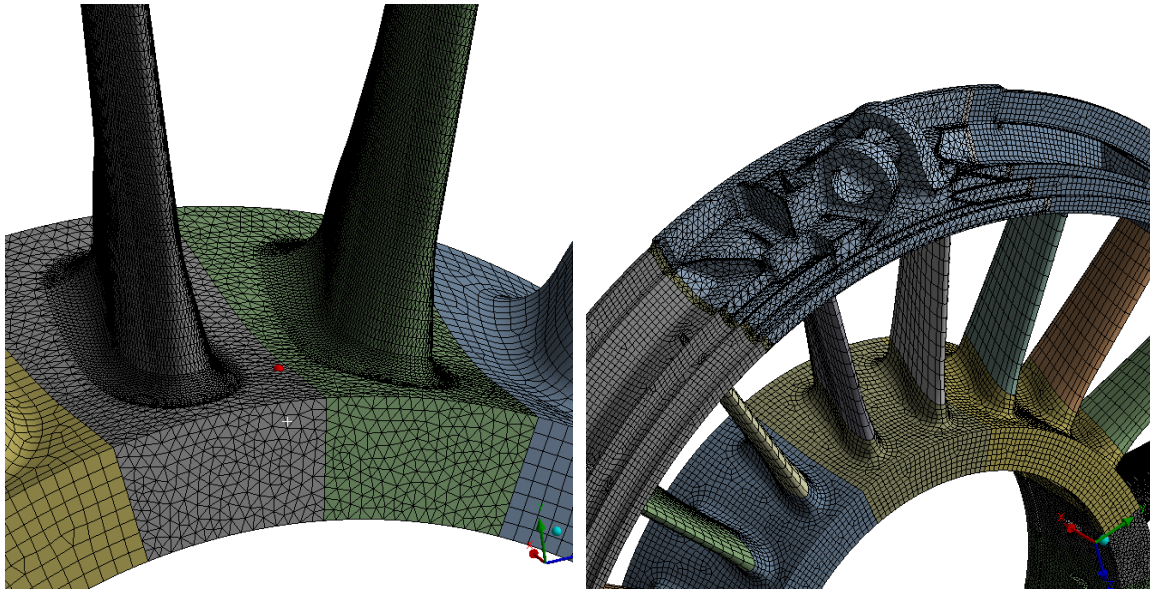
Fig 3.11 Mesh details in Ansys WB

At the latest step before loading the FE mesh, mesh compatibility between volumes are checked if the contacts will work properly. Also initial penetration between contact faces is checked. An example for the contact definition is given in Fig 3.12. Between the area shown in blue in Fig 3.13 and area in red in Fig 3.14 surface to surface contact elements are defined automatically.
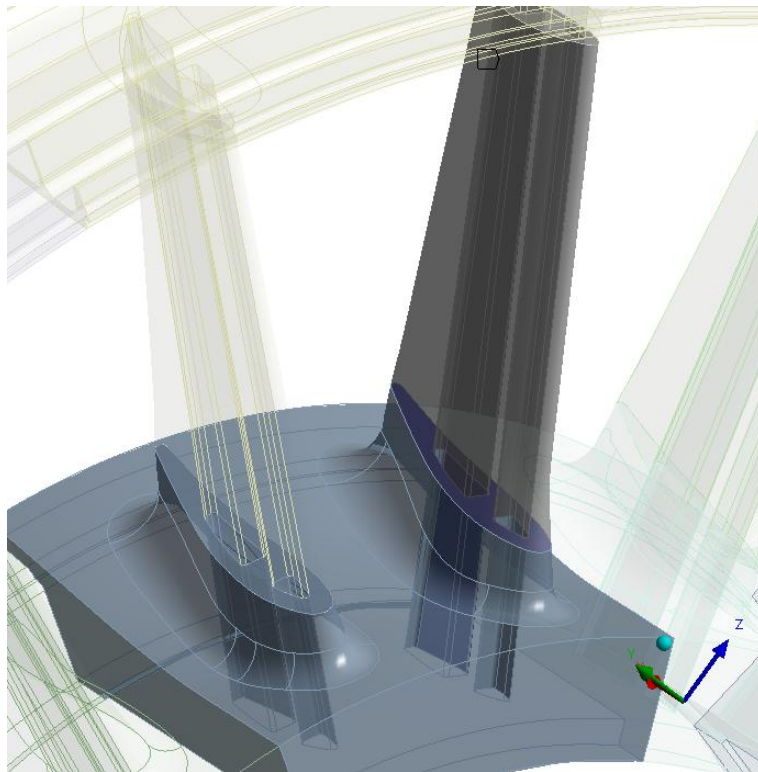
Fig 3.12 Example of contact definition
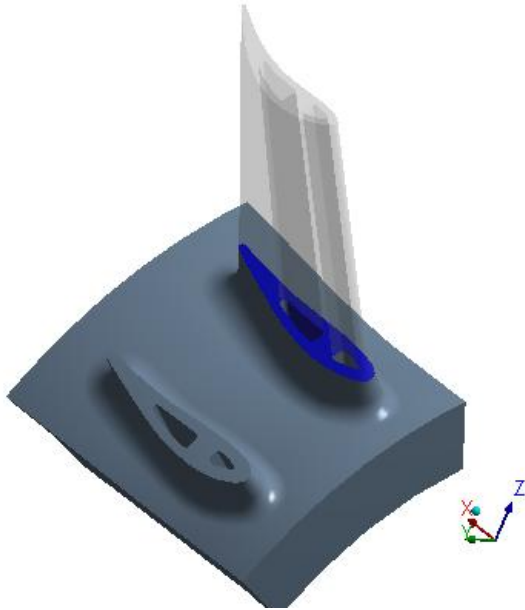
Fig 3.13 Contact area defined   **Fig 3.14** Target area defined
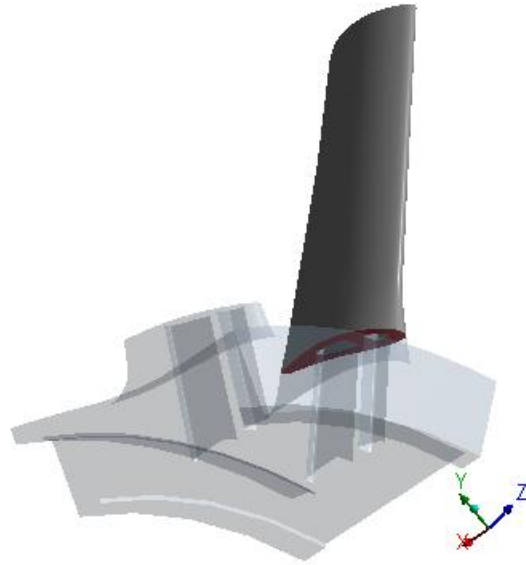
3.3.3 Load Definition and Loading Details

3.3.3.1 Load Definition:

The model is under different loads coming from different sources. At the end of the central tube, the total bending moment is applied, M_x, M_y, M_z. On the lugs, the forces applied are coming from the engine bars. Also on the front bearing centre axial force is applied. All applied temperature is 20℃.

This equivalent load definition for fatigue test is developed as follows;

- The missions having the biggest contribution to the total damage are defined for the selected life critical locations.

- To identify the behavior and the peak stresses, stress profile is plotted for the selected mission in previous step.

- The loading used in FE model and the test is obtained to meet the peak stresses at related locations.

Approximated values are defined as follows, Table 3.5:

Table 3.5 Equivalent load cycle

Definiton	Axial Force (N)	CT/FBS Mx (N.mm)	CT/FBS My (N.mm)	CT/FBS Mz (N.mm)	PORT (N)	STBD (N)
Equivalent Mission	-3,453E+04	-5,633E+06	-3,357E+03	-3,043E+07	-1,334E+05	5,198E+04

3.3.3.2 Load Application

In Ansys model, mass21 elements are only used as force application points. Only one real constant is defined in model to define the mass on point elements to zero. Nodes of these elements are master nodes for RBE3 connections. Applied force or moment on master node is distributed by RBE3 to a set of slave nodes. RBE3 takes into account not only the geometry of the slave nodes but also weighting factor which can be defined easily. RBE3 connections are working by defining constraint equations between the master node and the slaves. The applied force on master node is distributed to the slaves proportional to the weighting factor. As well as the forces applied, the moment is distributed as forces also. Distribution proportion is defined by the distance from the centre of gravity of the slave node times weighting factor. To construct the constraint equations, only the translational DOFs of the slave nodes are used.

To define some relations between nodes, Ansys basically introduces two terms: couplings and constraint equations. They both define a linear relationship between nodal degrees of freedom. While a couple between two nodes defines a simple relationship like (3.1), constraint equations are more general form of couplings and can be written as (3.2).

$$DOF1 = DOF2 \tag{3.1}$$

$$C1 * DOF1 + C2 * DOF2 + \cdots + Cn * DOFn = C \tag{3.2}$$

For couplings, even they can be defined for many nodes; they constrain only one degree of freedom. But a constraint equation gives user the privilege to use any number of nodes and any combination of degrees of freedom. In a model, they both have no limitations to the number can be defined.

Common applications for constraint equations in FE modeling are; connecting dissimilar meshes or element types, creating rigid regions and providing interference fits.

On the FE model one constraint equation is defined at the end of central tube and another one is defined on the front bearing support for load application. Defined constraint equations are shown below, in Fig 3.15.
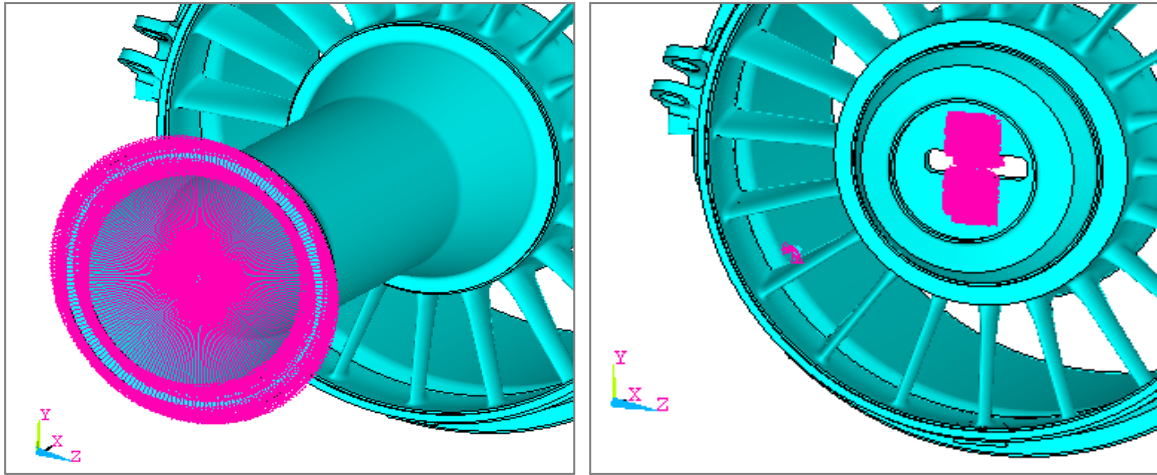
Fig 3.15 Constraint Equations on FE model

The moments and the axial forces are applied on these mass elements and the fixity is defined by assigning DOF values zero at the end of intermediate pressure case in Ansys as follows, Fig 3.16-18. The bearing loads are applied on an 120 degree circumferential section of the inner lug area sinusoidally. It is also given in Fig 3.19.
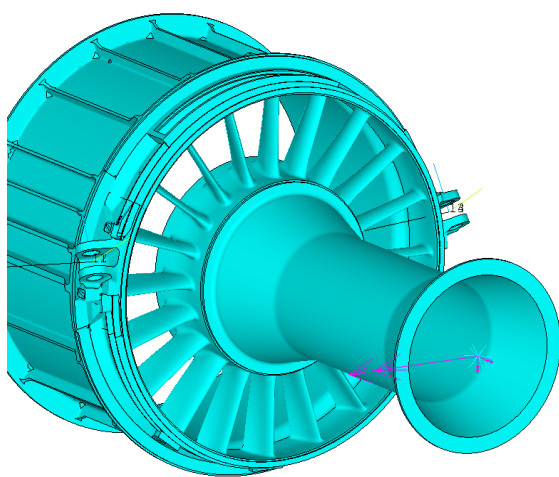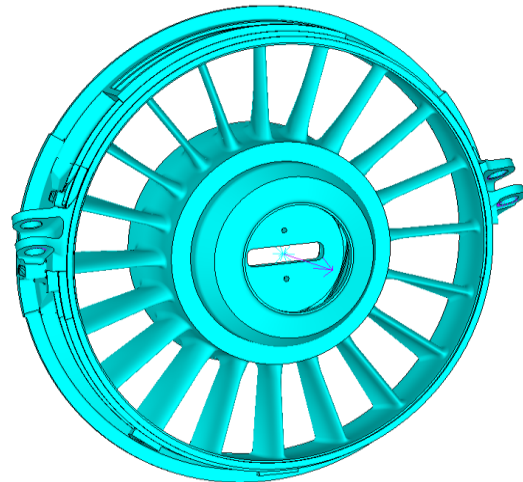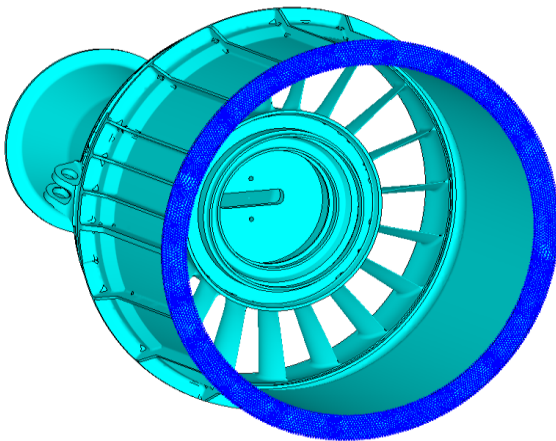

Fig 3.16 Moment applied on CT

Fig 3.17 Forces applied

Fig 3.18 DOF applied on IPC
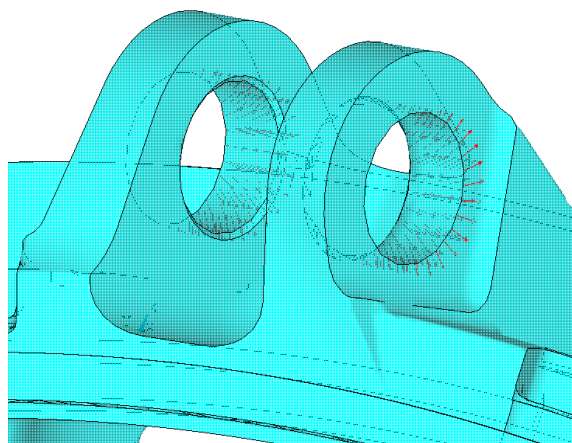
Fig 3.19 Bearing loads applied in lugs

41

In Ansys WB, there is a more practical way to apply loads and DOFs: All of them are being applied on the model via areas.

The applied loads to the FE model in Ansys WB can be found in Fig 3.20.
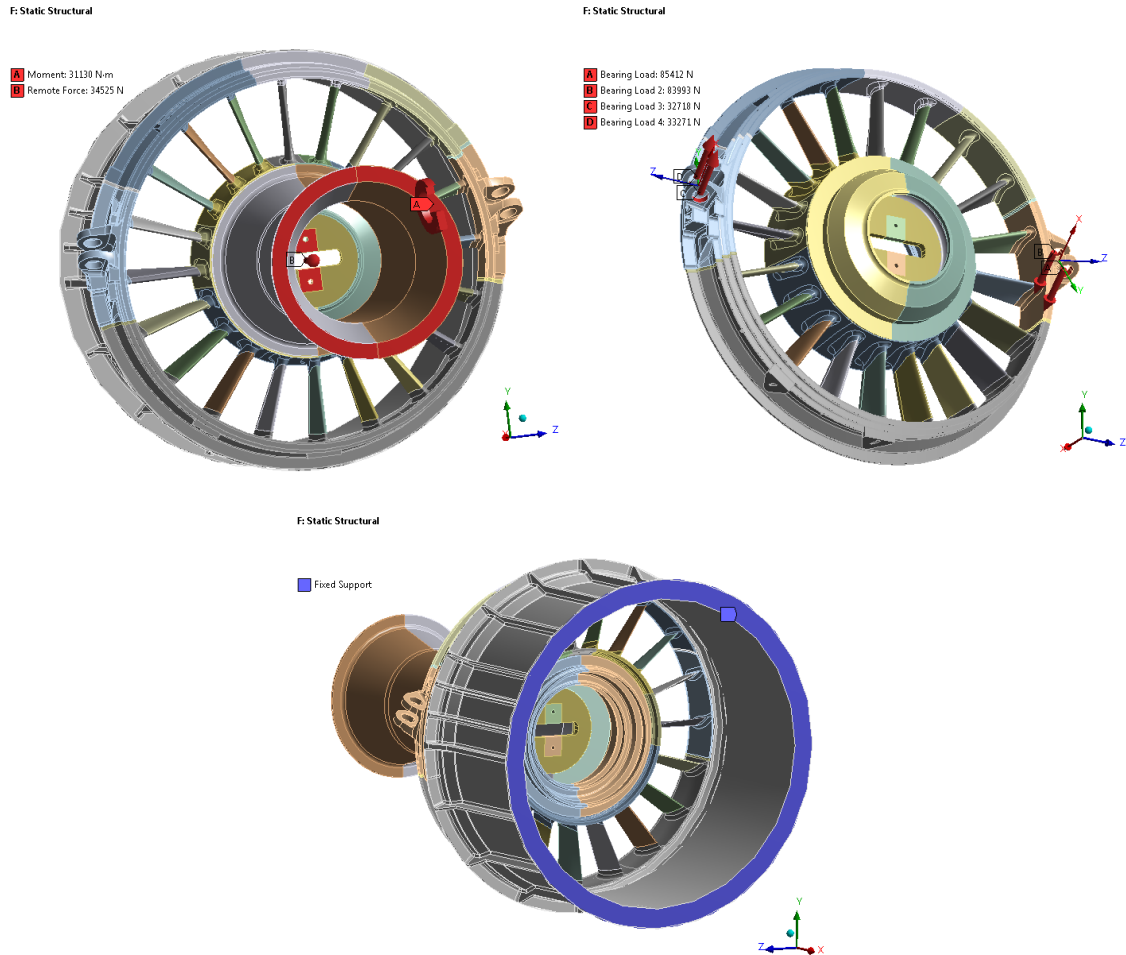
Fig 3.20 All loading on Ansys WB model

Both models in Ansys and Ansys WB are solved with the same solver named as Sparse Direct Solver.

3.3.4 Comparison of Results

In this part, the results of the static models in Ansys and Ansys WB are compared. Since fatigue and crack propagation analysis will be built on the model prepared with Ansys WB, its results should be consistent with the results evaluated from Ansys model which has been already validated with static test data.

All results are evaluated for the area of interest which is mainly Front Frame vanes in this part. The most effective loading on the model is *bending moment, M_z*. So, the max Equivalent Stress and the most effective principal stress, Third Principal Stress

(Compression) on the models are expected on the set of vanes #10-11-12, most probably on vane #11. All stresses are calculated based on the strain values. Hence, to be compliant, firstly the total deformation should be checked on the front frame. The max total deformation is given in Table 3.6. The comparison plots related to the total deformation is shown in Fig 3.21-22. (The plot contours are same.)

Table 3.6 Total deformation results

	Ansys	**Ansys WB**
Usum (mm)	0.73257	0.72662
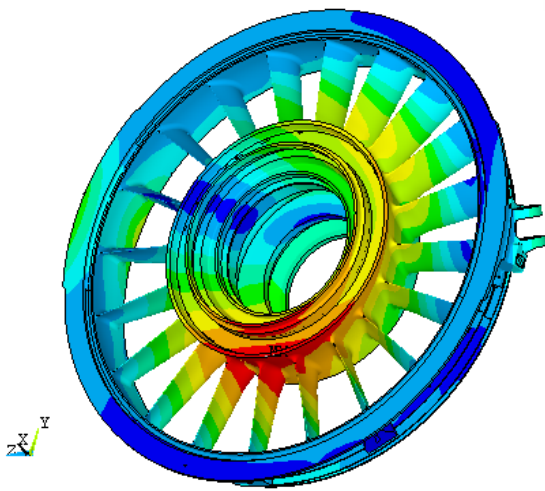
Fig 3.21 Total deformation (Ansys)   **Fig 3.22** Total deformation (Ansys WB)
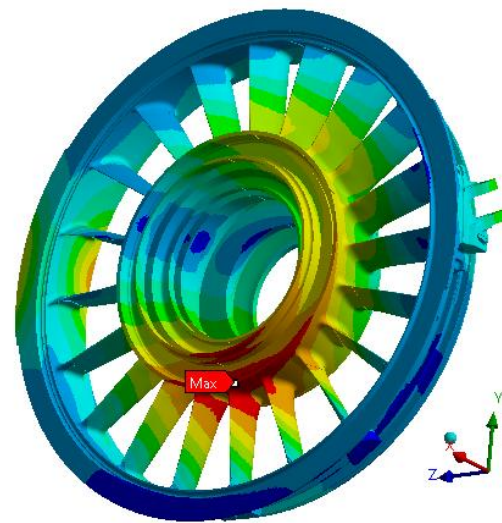
Total deformation locations are nearly the same, on the aft side of the inner ring of the front frame, circumferentially between the vane #10 and #11 as shown. Total deformation value in Ansys is approximately 6 microns higher than Ansys WB which is quite a good match.

For further check, the results between Ansys and Ansys WB, one location where the max S_{eqv} occurred is selected and compared. It is seen on vane #11 and the results are compared in Table 3.7 and the plots related to this table are given in Fig 3.23-24.

Table 3.7 Stress results comparison

	Ansys	**Ansys WB**
Seqv (MPa)	598.2	608
S_1 (MPa)	480.4	492.3
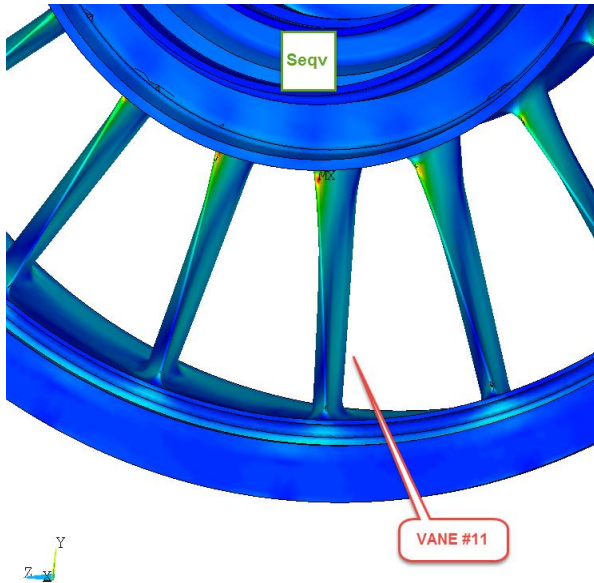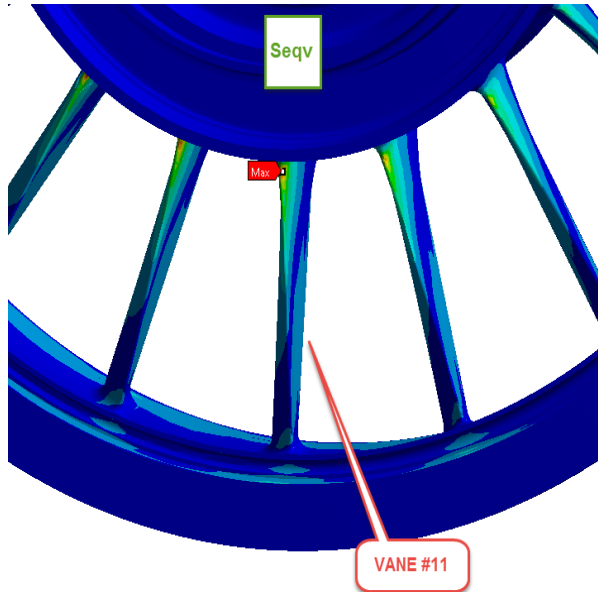
Fig 3.23 S_{eqv} (Ansys)   **Fig 3.24** S_{eqv} (Ansys WB)

The max S_{eqv} occur where expected on vane #11. The calculated error in equivalent stress based on Ansys is nearly 1.6%.

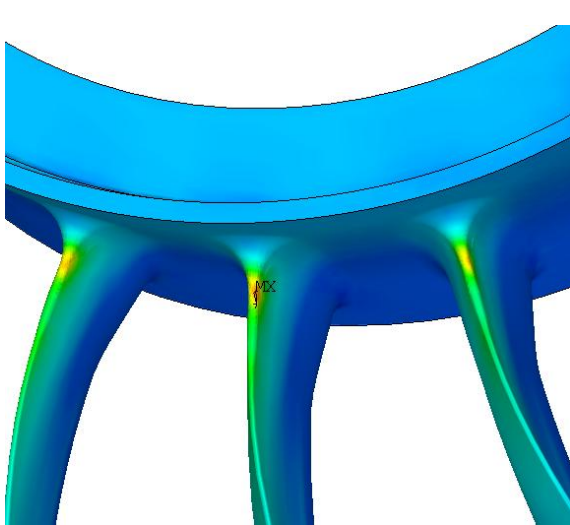Also the max principle stress S_1 occurs on vane #11 as shown and results tabulated in Table 3.7.
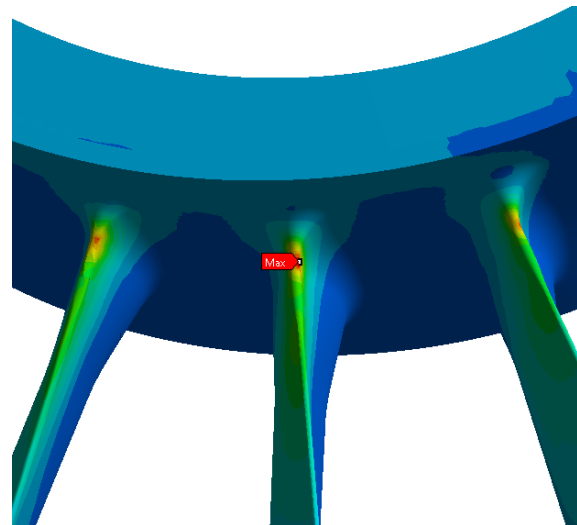

Fig 3.25 S_1 (Ansys)   **Fig 3.26** S_1 (Ansys WB)

Total deformation and related stress values are consistent between the two models. Deformation matches in a tolerance 6 microns at the same spot on the model and stresses show less than 2% error for the max location. In the light of these results, it is appropriate to proceed to further analysis with the model prepared in Ansys WB.

3.4 Fatigue Analysis with ANSYS Workbench

Life prediction is performed on the model and static structural analysis results explained in previous section with the *strain-life* methodology which is based on strain-life relation is used explained in details in previous chapter. Required strain-life parameters are shown below.

Table 3.8 Strain-life and cyclic parameters [9]

Strain-Life Parameters	Titanium Alloy
σ_f' (Mpa)	809,4
b	-0,0777
ε_f'	0,9486
c	-0,7363
K' (Mpa)	1510
n'	0,1

The model is loaded with constant amplitude and the loading is zero based, R-ratio=0. Loading history is shown in Fig 3.27. X-axis is time and y-axis is unit loading.
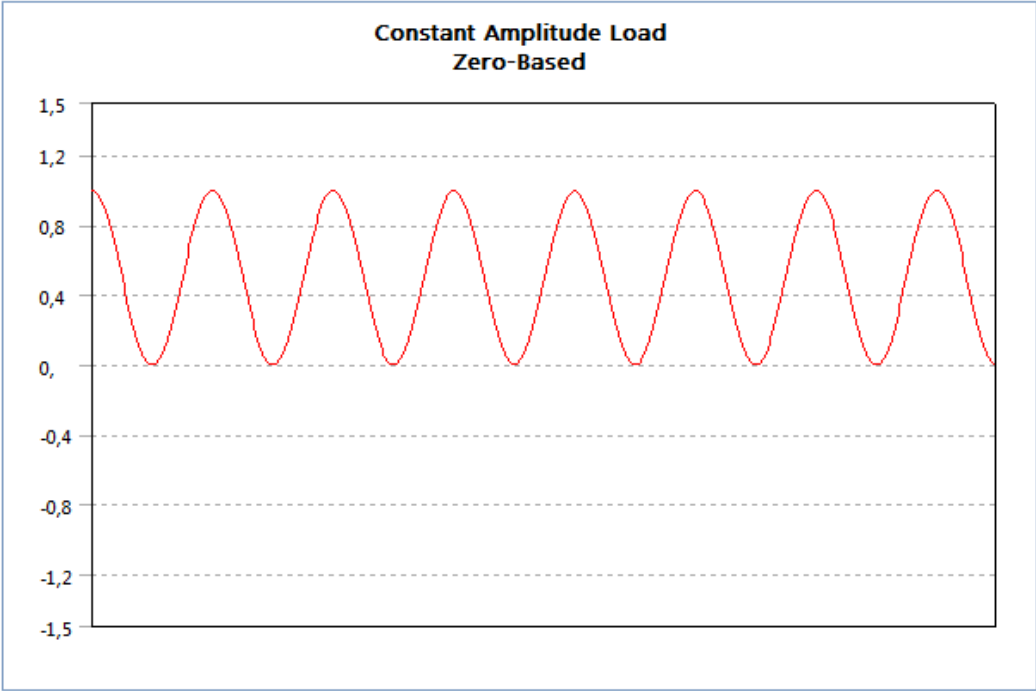
Fig 3.27 Loading history of fatigue analysis

As mean stress correction theory Morrow is preferred. The related base strain-life curve and corrected curve is given below.
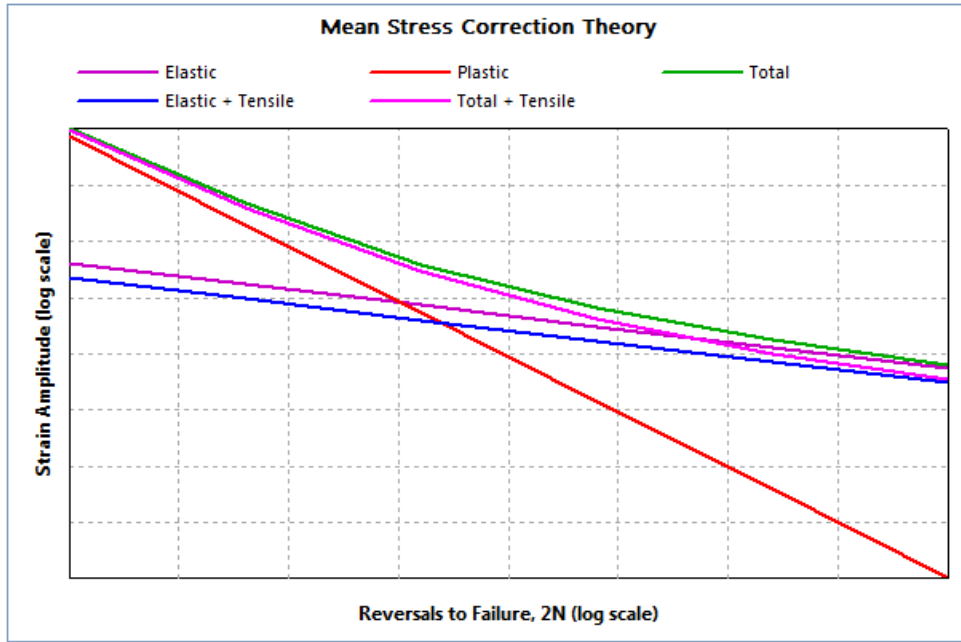
Fig 3.28 Mean Stress Correction Theory

3.4.1 Life Results

To predict the life results, the results from static structural analysis are used. In Ansys WB, a tool is very helpful to get the results easily named as *'fatigue tool'*. Life prediction on the FBS front frame is given in Fig 3.29 in contours related.
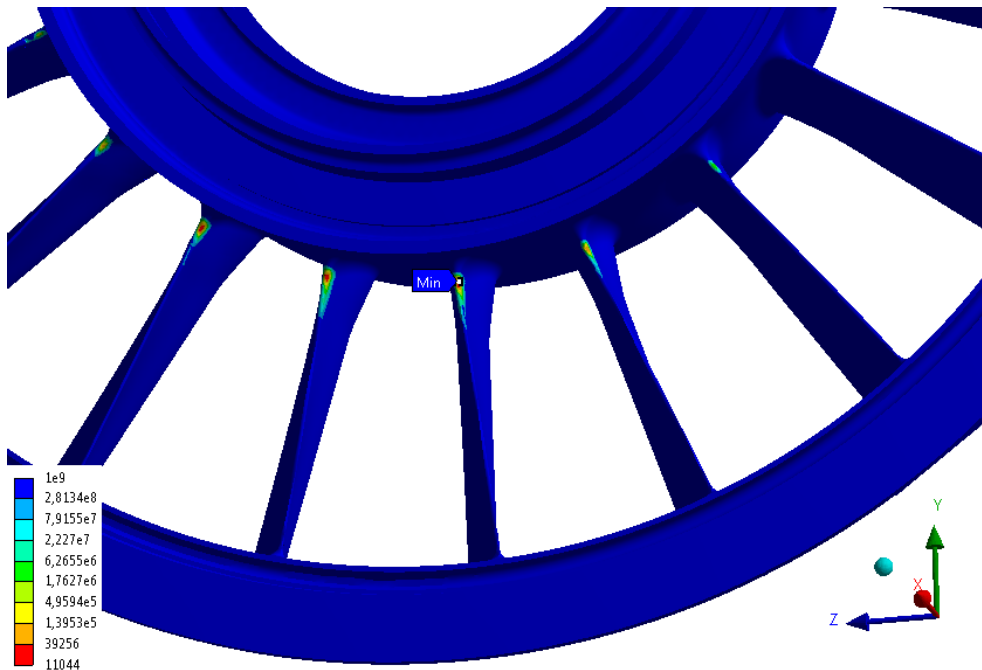

Fig 3.29 Life prediction results

The life results gives that the min life value on the front frame is nearly 11000 cycles and it is observed where the max principal and equivalent stress occurred. It is

important to remember that strain-life methodology predicts the life cycles in phase crack initiation.

3.5 Crack Propagation Analysis

The most effective loading on the model is *bending moment, M_z*. So, the crack initiation on the model is expected on the set of vanes #10-11-12 where the max principle stress S_1 occurs. But the first initiated crack on the FBS occurred on vane #20. Even the FPI results show no initial defect on the part before test, it is thought there was a notch on the part smaller than the tolerance of FPI.

Since the crack on the test is grown on vane #20, it is decided to move the crack location for these analyses from vane #11 to vane #20. On vane #20, max principle stress location is selected as the location where crack will start from. Vane numbers is shown in Fig 3.30.
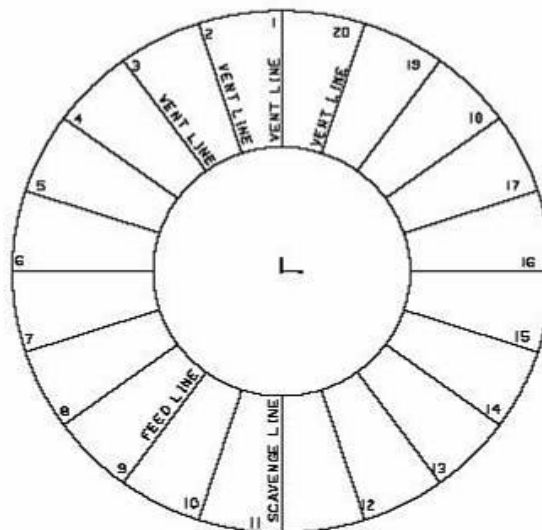
Fig 3.30 Vane numbers on FBS

After fixing the location where crack will be implemented, the path of the crack is monitored and it is seen it is growing parallel to surface which is normal to vane normal. Also vane is cracked equally on both sides of the vane.

3.5.1 Crack Modelling

Because of having holes inside the vane which cause separate surfaces during the crack face, original Ansys WB tool which helps to implement a crack on geometry surfaces did not work for bigger than 1mm cracks. Hence, to solve this problem and to be ready to analyze different crack lengths, parametric crack length is defined by using the geometry. Also having these holes is forced this study go on for three

different parametric models. Section of the vane and related lengths for parametric models are shown in Fig 3.31. Except the crack lengths, there is no difference in the models.
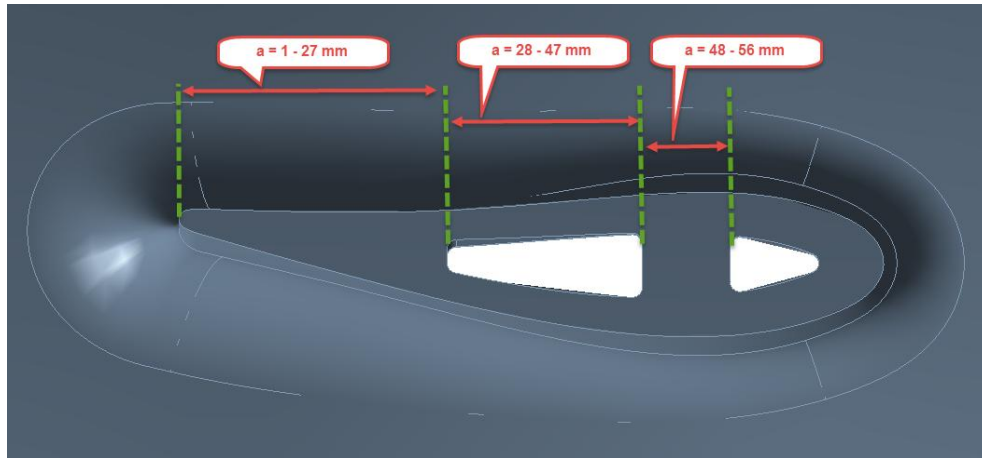

Fig 3.31 Intervals defined through crack length

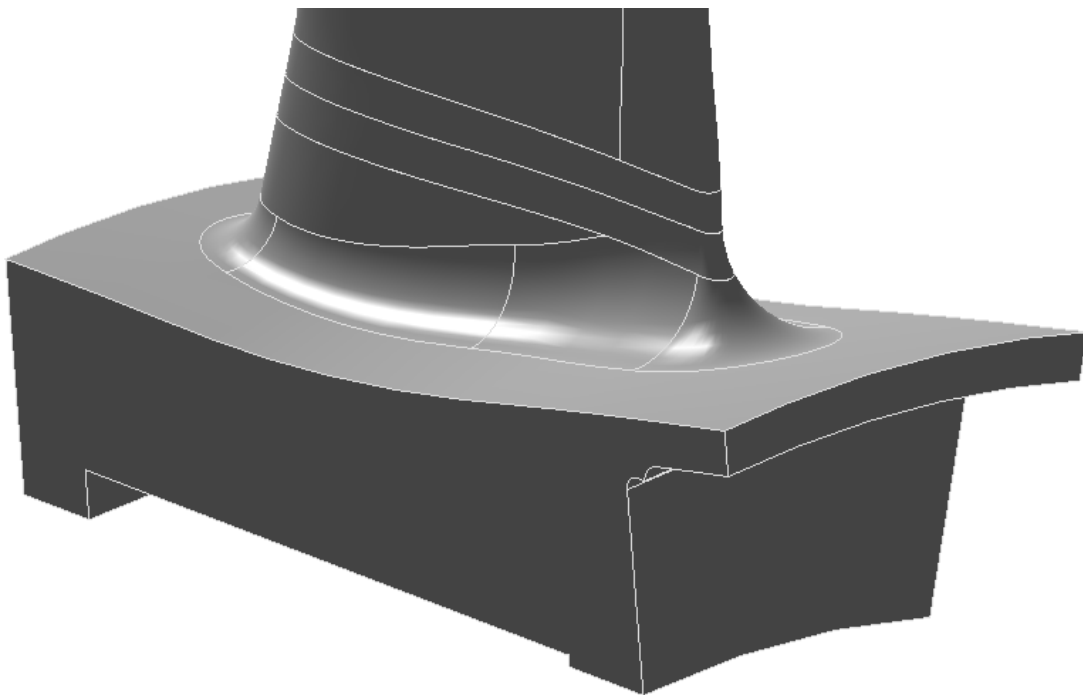Geometry of the inner root of vane #20 where crack will be located is updated as shown in Fig 3.32.

Fig 3.32 Geometry of the cracked vane

J-integral fracture criterion is used for study and Ansys WB provides J-integral values for the crack tip via *'fracture tool'* which can be defined in `Solution` easily. In order to use this tool, a crack should have been defined before starting solution. Since the crack implementation is not manageable by defining the available cracks in

'Modeling', Ansys WB offers another way named as *pre-meshed crack*. It gives proper results if the crack area is meshed with hex elements. [16] Hence, the mesh built for previous analysis is reserved for the geometry except the crack located vane. The mesh built for the vane #20 is shown in Fig 3.33.
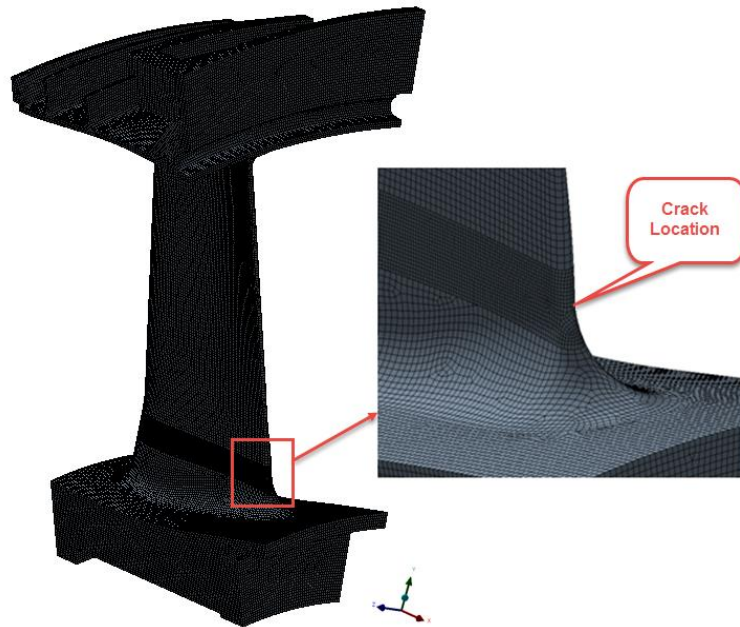

Fig 3.33 Mesh details of the cracked vane

Fracture Properties for Ti-6Al-4V: Crack propagation curve of Ti-6Al-4V whose fracture toughness is defined as K_{Ic}=47.4 MPa.m$^{1/2}$ is given.
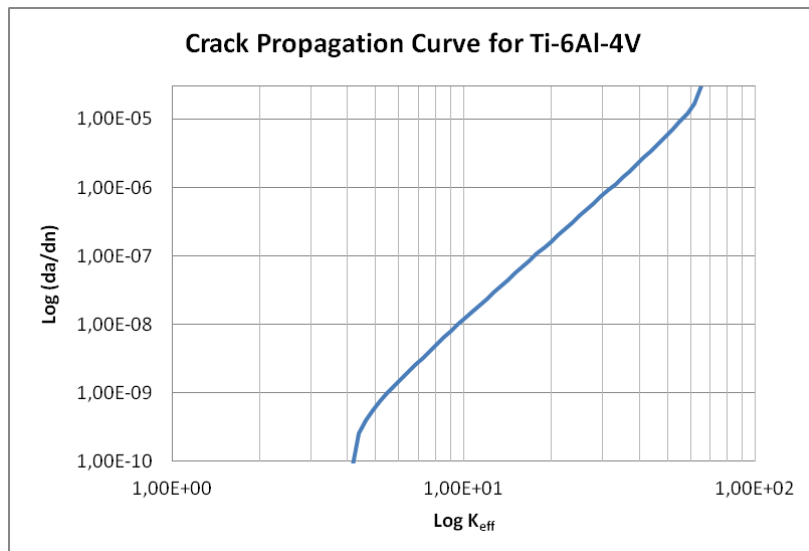
Fig 3.34 Crack growth rate according to stress intensity factor, K_{eff}

Critical J-integral value is determined as

$$J_c = K_{Ic}^2 \left(\frac{1 - \vartheta^2}{E} \right) = 4178.974 \frac{J}{m^2}$$

(3.3)

The models are solved for the crack lengths given in the Table 3.9.

Table 3.9 Case numbers and crack lengths

Case #	1	2	3	4	5	6	7	8	9	10	11	12	13	14	15	16	17	18
a (mm)	1	3	5	7	8	11	15	18	20	23	25	27	30	34	39	42	47	51

3.5.2 Analysis Results for Case #3 - 5mm Crack Length

Results of an example case #3 run is given to provide information about how the cracked vane deforms and what types of stresses accumulate on the vane.

Total deformation of the vane #20 is shown, Fig 3.35. While at the outer surface of the crack max total displacement is nearly 0.433 mm, at bottom surface it reaches out to 0.45mm.
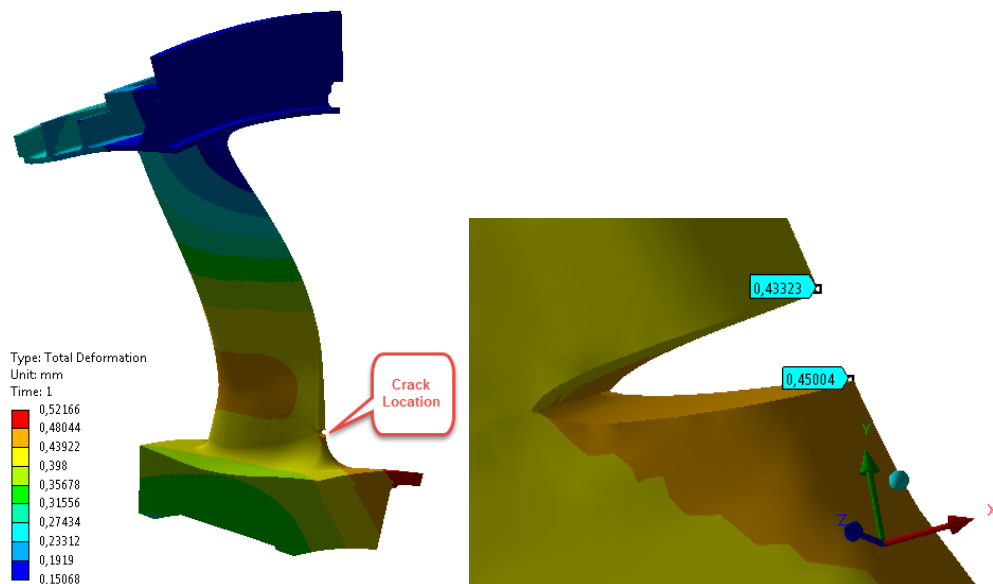

Fig 3.35 Total deformation on cracked vane

When the stress levels on vane is checked, an understandable increase in equivalent stress is observed. Without any crack on the vane (Fig 3.36) S_{eqv} is evaluated as 388 MPa but in cracked vane (Fig 3.37) there is an accumulated stress at tip of the crack nearly 821 MPa. Stress distribution on vanes can be seen below
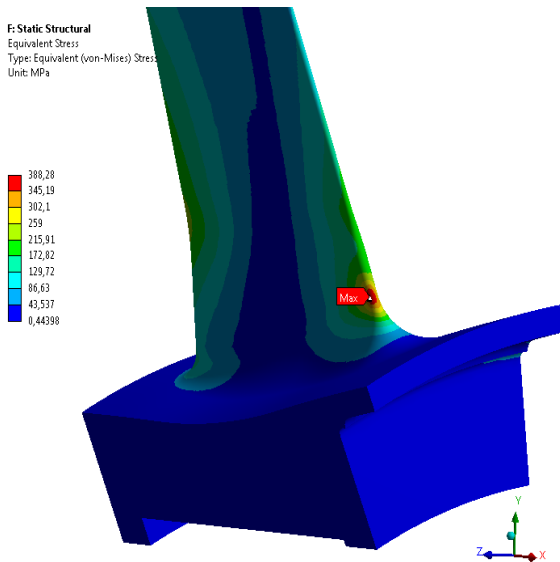
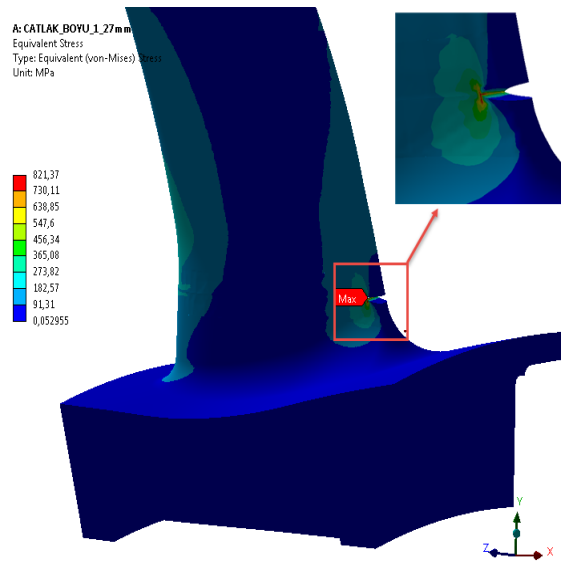**Fig 3.36** S_{eqv} on the vane w/o crack   **Fig 3.37** S_{eqv} on the vane near crack

Finally the *stress intensity factor, K1* and *J-integral* plots of the cracked vane are shown in Fig 3.38-40. Maximum J-integral value at crack tip is 6483.2 J/m^2, since maximum K1 along the crack tip 25.92 MPa.mm$^{1/2}$. These values are given from the maximum location through the crack length.
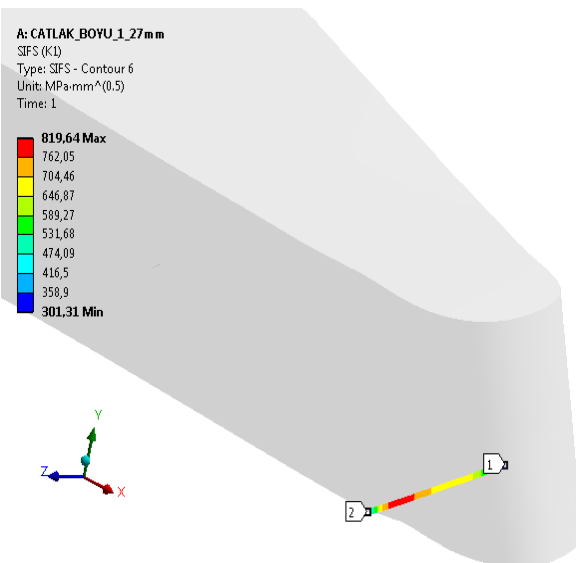

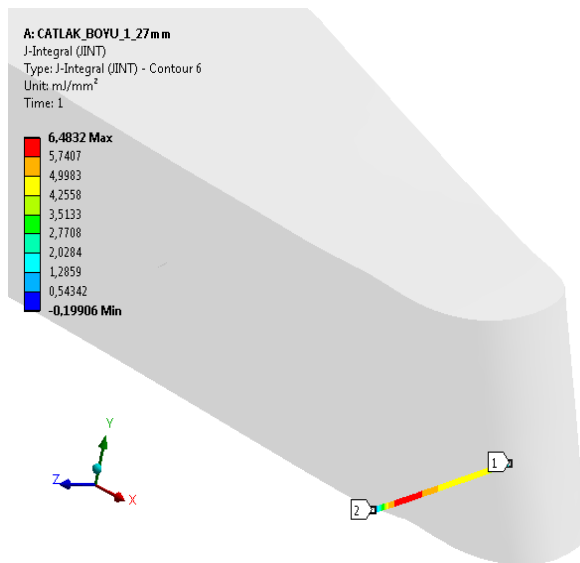**Fig 3.38** Mode-I K through the crack tip   **Fig 3.39** J-integral through the crack tip

3.5.3   Run Results with Implemented Crack for Different Lengths

The calculated critical J-integral value, J_c is equal to 34166 J/m^2 for Ti-6Al-4V. It can be seen in Table 3.10 that all J-integral values are below the critical J-integral value. Hence, it can be stated as the crack growth is in the Region-2 which behaves in a manner of stable and predictable growth.

Table 3.10 J-integral values for different crack lengths

a [m]	J-int [J/m^2]
0,001	893,1
0,003	5559,7
0,005	5599,9
0,007	5806,2
0,008	4473,2
0,011	3879,3
0,015	3224,4
0,018	2959,6
0,020	2942,7
0,023	3143,3
0,025	3787,5
0,027	4958,7
0,030	4961,3
0,034	3164,2
0,039	1096,0
0,042	1104,2
0,047	298,4
0,051	156,7

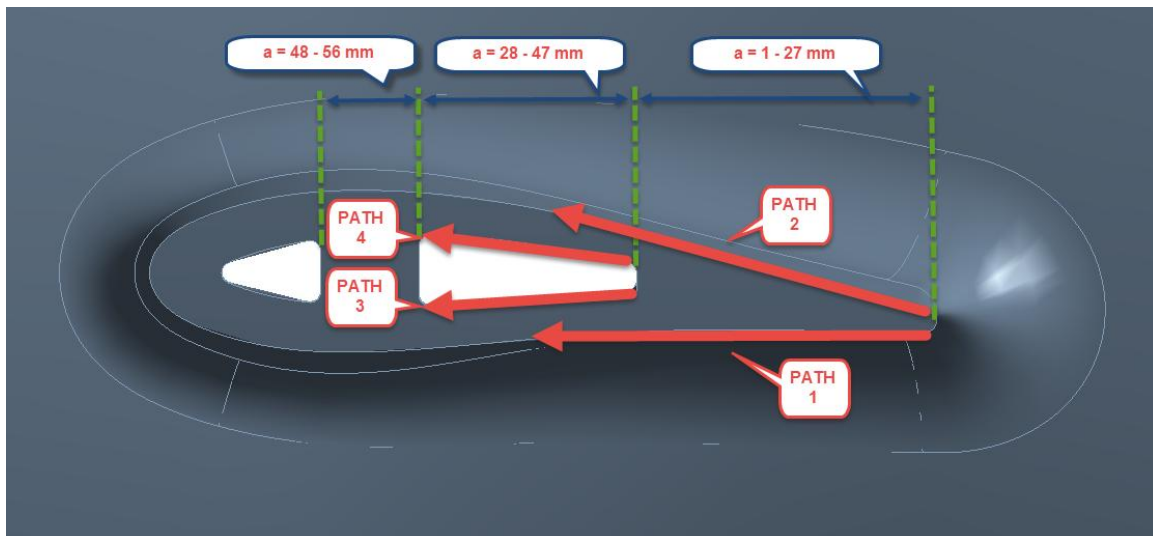On the edges of vane, different crack paths are defined through the crack plane as shown below.

Fig 3.40 Defined paths on crack edges

On defined paths, related stress intensity factors and J-integral values are gathered; details of paths are given in Appendix A. The comparison of the stress intensity factor, K_I between the paths according to crack length,a is shown in Fig 3.41. To proceed with, path-1 where the max K_I is observed is selected.
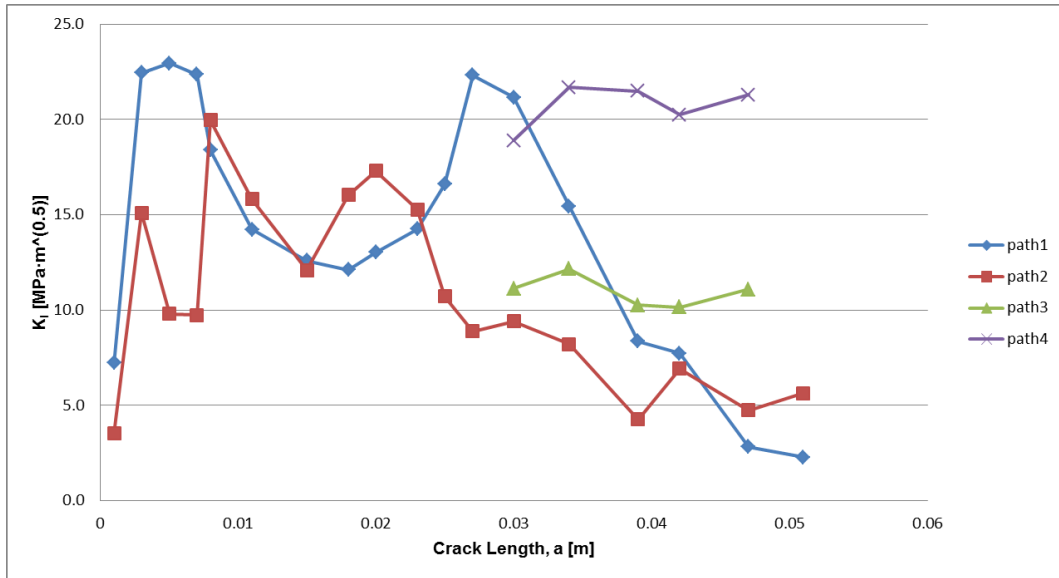
Fig 3.41 Defined paths on crack edges

Stress intensity factor levels related to Path-1 is given below in Fig 3.42. K_I is the main component with respect to K_{II} and K_{III}.
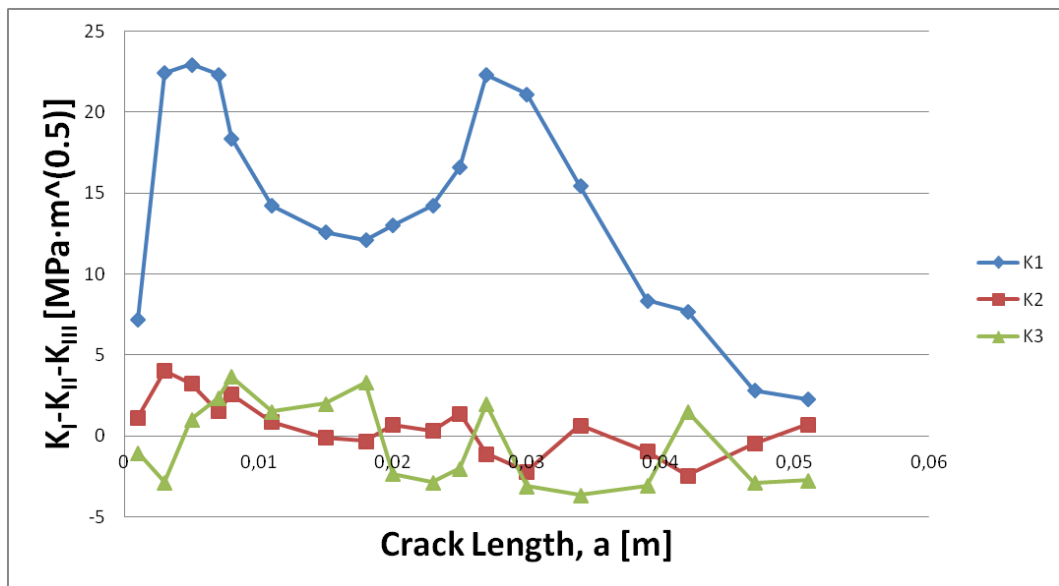

Fig 3.42 Stress Intensity Factors through Path-1

Hence, it is suitable to apply Paris-Erdogan's Law which is shown below, to find the number of cycles needed for related crack lengths.

$$\frac{da}{dN} = C\,(\Delta K\,)^m \tag{3.4}$$

Since ΔK is a function of crack length, a sixth degree polynomial curve is fitted via regression.
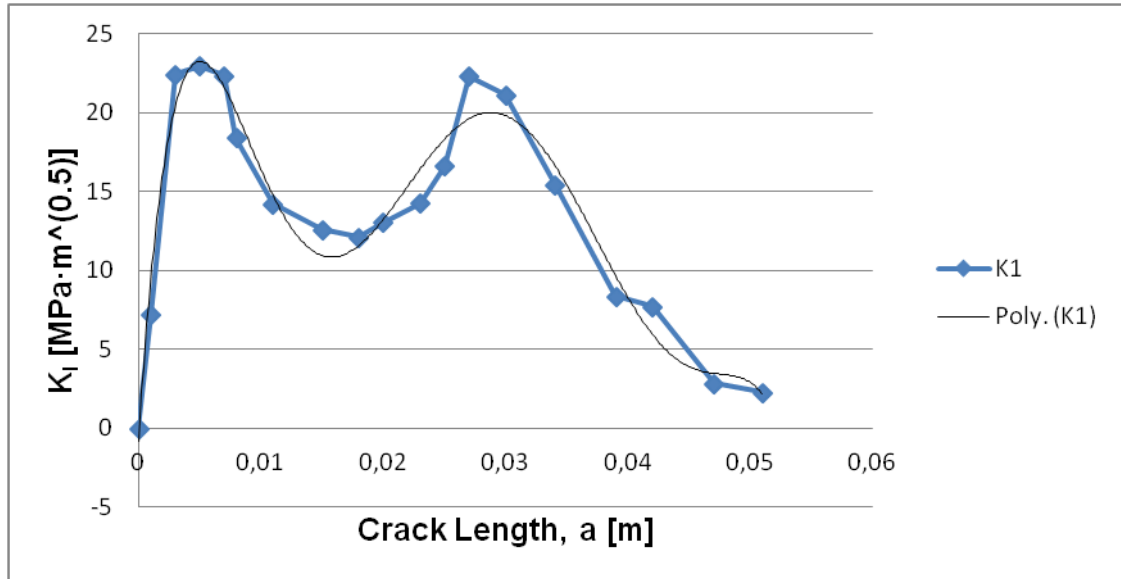
Fig 3.43 K1 through crack length and fitted curve

$$y = C_1 * x^6 + C_2 * x^5 + C_3 * x^4 + C_4 * x^3 + C_5 * x^2 + C_6 * x^1 + C_7 \qquad (3.5)$$

Table 3.11 Constant values for the polynomial fit

Coefficient	Value
C_1	-383.917.151.245,75
C_2	66.812.333.026,54
C_3	-4.429.062.599,90
C_4	138.328.098,45
C_5	-2.035.240,22
C_6	12.045,88
C_7	-0,83

The C and m constants are taken as below [17],

$$C = 3.80 * 10^{-11} \qquad (3.6)$$

$$m = 3.11 \qquad (3.7)$$

The equation to calculate number of cycles needed is as

$$n_f = \int_0^{n_f} dn = \int_{a_0}^{a_c} \frac{da}{C(\Delta K)^m} \qquad (3.8)$$

This equation is numerically solved via Matlab in upper and lower boundaries of crack length from test data, 12 mm and 39.6 mm respectively. The intervals are

chosen with respect to measured test intervals. The number of cycles needed is shown in Fig 3.44.
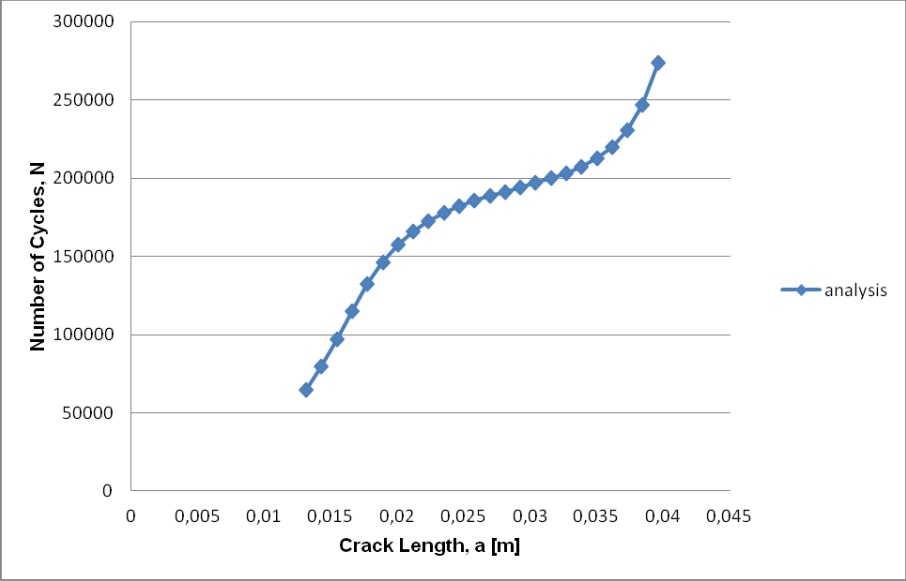

Fig 3.44 Number of cycles vs crack length

# 4   LCF FATIGUE TEST AND COMPARISON WITH THE ANALYSIS

The test data covers a fatigue test performed with FBS. This test is required to demonstrate the fatigue capability of hardware for fatigue load envelope defined previously. It was performed in accordance with the requirements defined which can not be exposed in here due to confidentiality of commercial property.

The test object FBS is delivered as ready for built without any painting or coating.

4.1   Test Rig Setup

Fatigue test setup is prepared with respect to test requirements. The test centre provided a dummy which is able to substitute the complete FBS - IPC - CT & BRG hardware. This dummy offers all the interfaces for actuators, bars and flanges. After tuning completed and all the control system parameters required are stored, the setup was ready for the test.

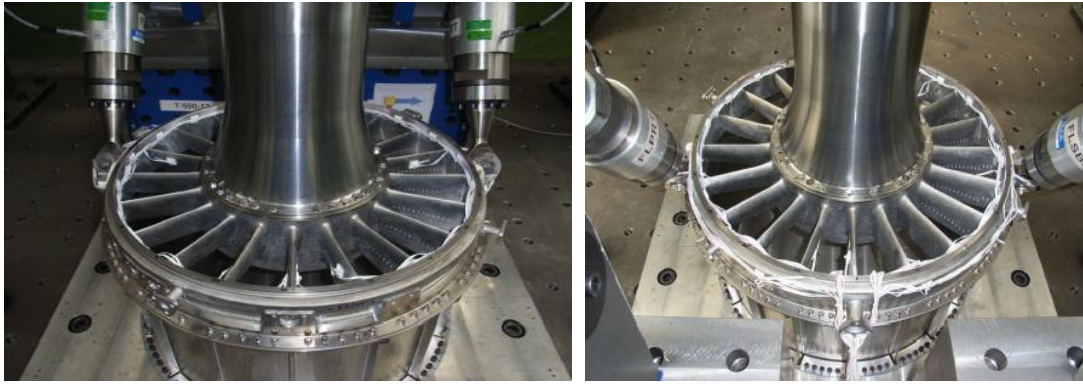Different views of the test rig setup can be found in Fig 4.1.
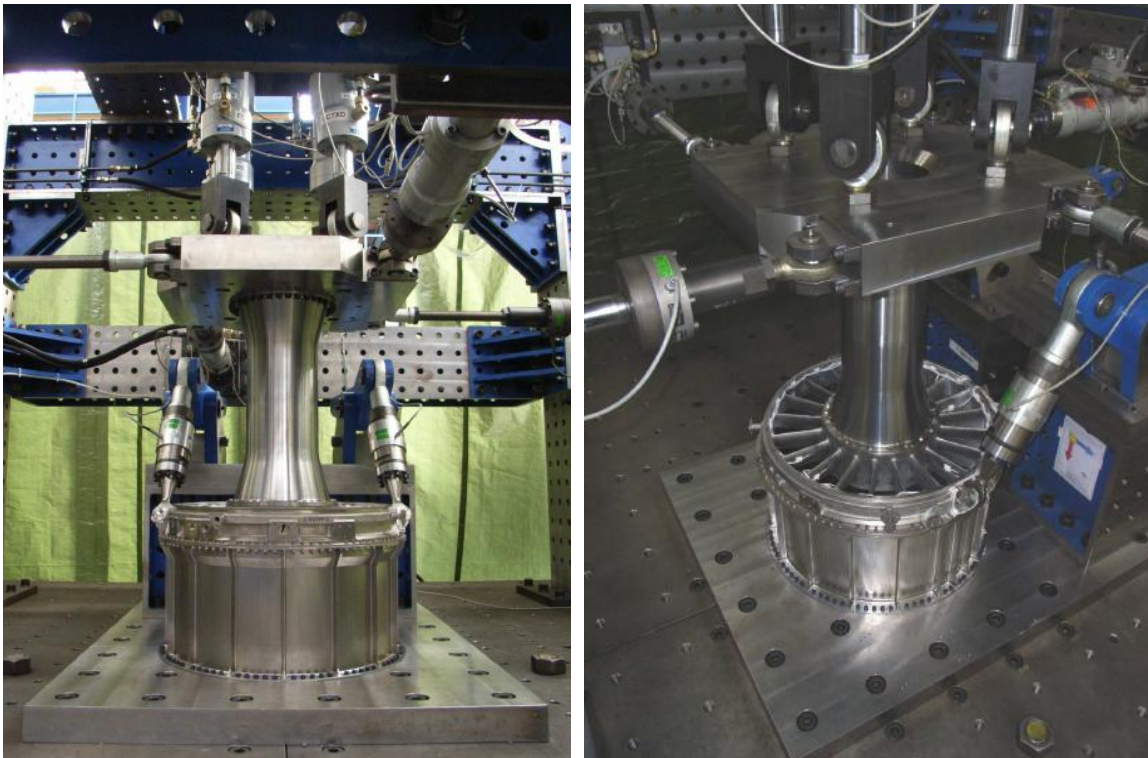
Fig 4.1 Different views of test rig setup

The test-article is required to be instrumented with strain gauges in order to measure data and to monitor the component during the test. (25 SG's at different locations)

A data acquisition system which is available to measure the total number of 35 channels exists. Load cells feedback signals and strain gauge signals were recorded and archived via using a data recording software. Also, there is a load control system which covers special hard- and soft-ware features for aerospace component testing. Its features provide protection to test article from overloading by controlling the servo-loops for each hydraulic actuator.

A total number of 25 single SG channels are available. Positive measured signals mean positive strain, tension on the part, while negative measured signals mean negative strain, compression on the part. A sample application of the strain gauge is shown in Fig 4.2.

Fig 4.2 Strain gauge application

4.2 Inspection

Three different inspections are applied during the test.

- Full FPI: Two full FPI's were needed on the component, before and after the fatigue test series, which carried out accordingly the European standard EN 571-1-ICs-5.

- Local FPI: On the built-in component, 6 FPI inspections were performed. Intervals between FPI's were defined on the number of load cycles. It was also performed according to European standard. In addition to test component FBS, the secondary test hardware IPC dummy was locally FPI checked.

- Visual Inspection: On the built-in test article, 16 visual checks were performed. Besides one inspection after finishing the fatigue cycling, other inspection timings are defined depending on the load cycles.

4.3 Test Procedure and Results

Prior to fatigue test; different pre-tests were performed for tuning the set-up. Also for final control, unitary load cases are tested on the component. Then, load application frequency is determined as 0.25 Hz for fatigue test, after examining the results for different frequencies.

Fatigue cycling: Fatigue test phase performed with respect to a defined test schedule. One load set contains a fatigue cycle and a data acquisition cycle. While data acquisition cycle was always 20 load cycles, fatigue cycle had number of cycles within the fatigue cycle varies over the course of fatigue test due to inspection requirements, from 3300 cycles up to 60000 cycles.

For fatigue testing only the fatigue load case LCF was used as continuously repeating. The loads were ramped-up from zero with all masses compensated. The loads were applied for all actuators simultaneously as trapeze profile cycle.

All inspections were performed at the end of each load set after data acquisition cycle.

The fatigue test 1 had completed 200k cycles as planned, and then it is decided to continue up to 280k cycles to observe the crack propagation on the vanes. The related FPI items of the fatigue test schedule are shown in Table 4.1.

Table 4.1 FPI schedule of the test

Load Set	Load cycle	Inspection
0	0	full FPI
1	9.1k	local FPI
2	12.4k	local FPI
4	25k	local FPI
10	80k	local FPI
14	124k	local FPI
17	160k	local FPI
22	280k	full FPI

Crack propagation: During the fatigue cycling, one crack was detected, on vane 20.

At the end of load set 14, (124k cycles) the crack, whose length is already 12 mm at both sides of the vane was detected during the local FPI on inner trailing edge of vane 20. Then it was decided to apply a crack gauge to observe the crack propagation behavior.

Crack gauge: The gauge contains a number of links or wires which are arranged perpendicular to the expected crack propagation direction. It allows observing and determining the crack propagation while the links are destroyed consecutively. The crack gauges applied had 10 links and the distance between links was 1.15 mm.

During the test (until 280k cycles), 3 crack gauges were applied on the vane 20. The installation of crack gauges can be found in Fig 4.3.
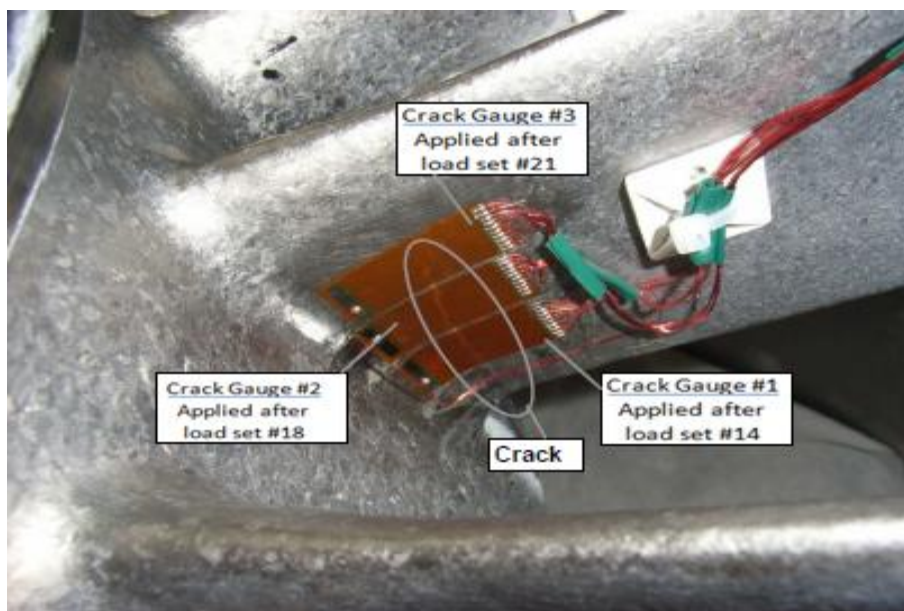

Fig 4.3 Crack gauge installation

After the installation of the first gauge, crack propagation is observed. After breaking the last link on the first gauge, second gauge was installed at the end of load set 18 (174k cycles). Third gauge was installed after the load set 21 (222k cycles) and used till the end of the fatigue test, 5 broken links. First two crack gauges' data is considered in this study. The cycles needed to break the links on crack gauges are shown in Fig 4.4.
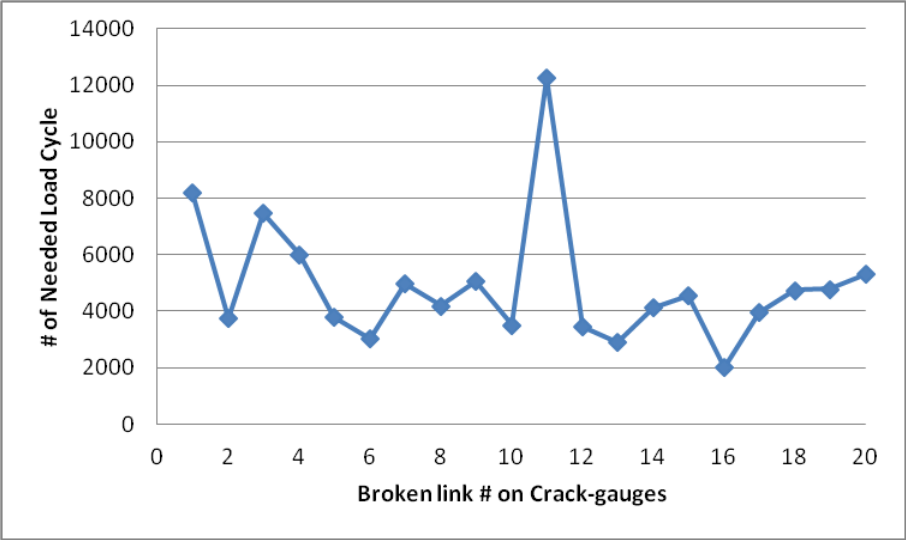

Fig 4.4 Broken link number vs number of load cycles

The median is found as 4375 cycles and the average value calculated as 4520 cycles without outsider point, 11 for Fig 4.4.

Crack length assumed from broken links of crack gauge is plotted with respect to number of cycles as
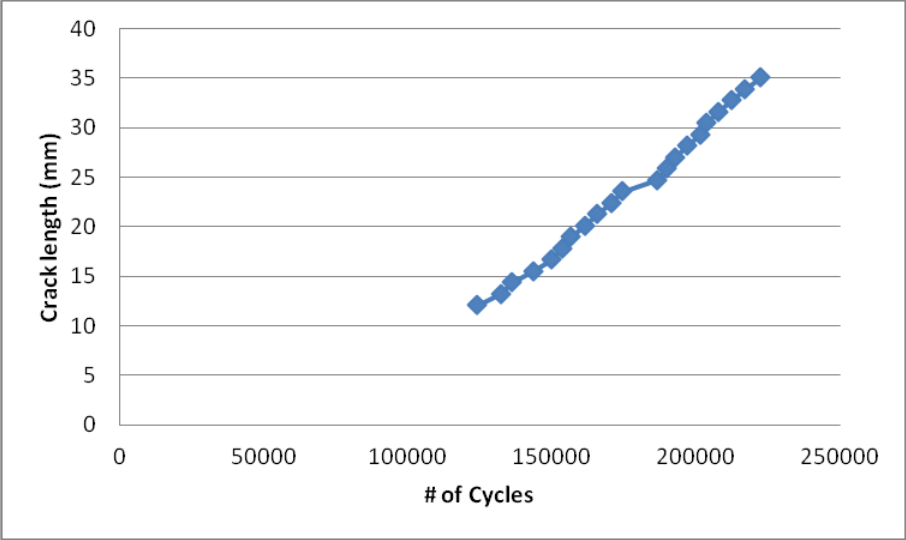

Fig 4.5 Number of cycles vs crack length

At the end of the fatigue test (280k cycles), the crack on vane 20 reached out app. 41mm. The FPI results and length of cracks is given in Table 2.

Table 4.2 Results of inspections

Load Set	Inspection	Result
0	full FPI	no indication
1	local FPI	no indication
2	local FPI	no indication
4	local FPI	no indication
10	local FPI	no indication
14	local FPI	1 crack in vane 20,
17	local FPI	crack in vane 20, length 18 mm
22	full FPI	1 crack in vane 20, length 41 mm

The crack on vane 20, during FPI inspections, after load set 14 and 18 are shown below in Fig 4.6 & 4.7.
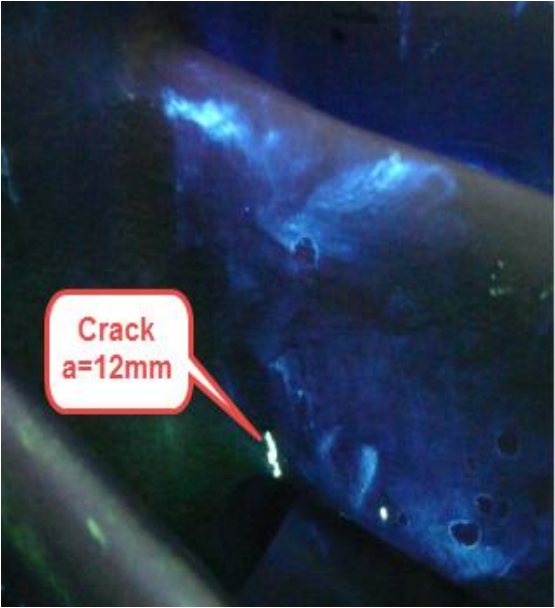

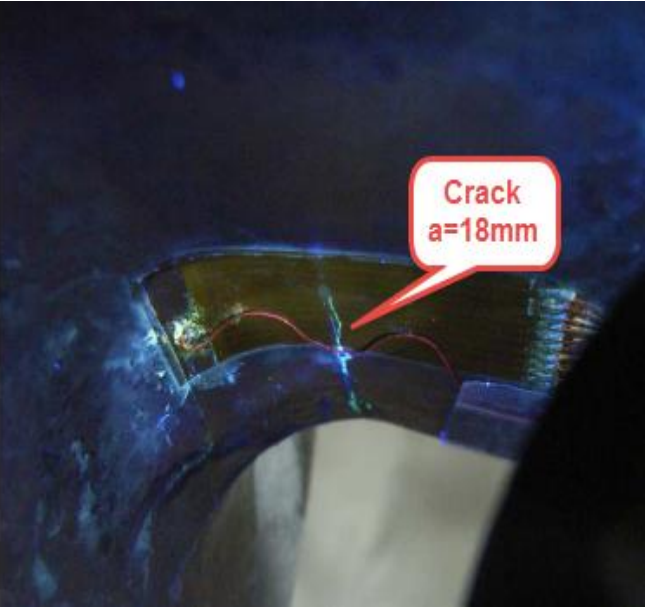**Fig 4.6** FPI result for load set #14   **Fig 4.7** FPI result for load set #18

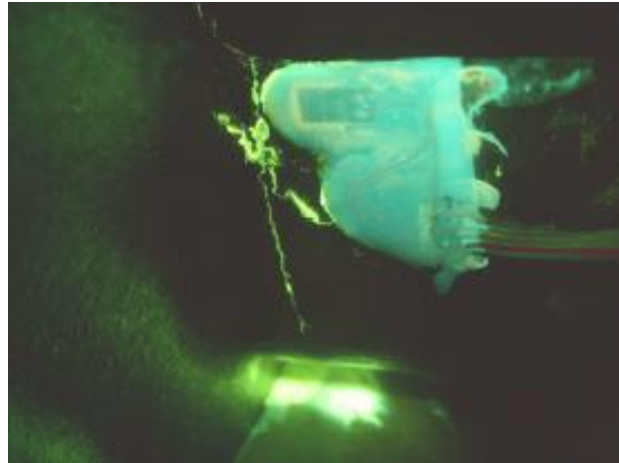At the end of fatigue test, the cracks observed are given in Fig 4.8.

Fig 4.8 FPI result of Vane #20

All the inspections during the fatigue test were restricted by strain gauges and cables. Also after application of the crack gauges, the crack length measurements are valid for only one side of the vane 20. The first measurement data from vane 20 (12mm at both sides) before the crack gauge installation was confirmed by eddy current testing.

4.4   Comparison between the Test and the Analysis

After defining the general behavior of the crack growth rate through increasing crack lengths by extracting ΔKs from the analysis, the number of cycles needed for determined crack lengths are evaluated for the interval defined from the crack gauges' links to make a comparison between the FE analysis and the test results.
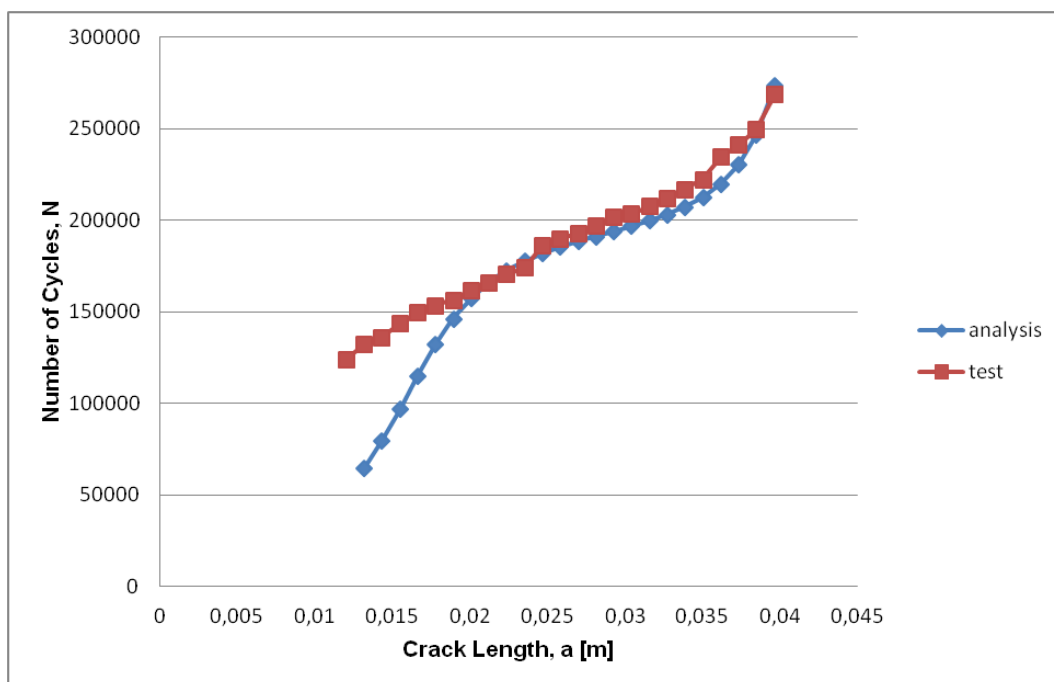

Fig 4.9 Comparison between the analysis and the test results

5 CONCLUSION

Low Cycle Fatigue (LCF) is one of mechanical failures commonly seen in components of gas turbine engines. The results of the failure might be catastrophic if it is not designed properly and monitored closely. In design phase of a component, LCF life should be checked and validated by component rig tests.

The object of interest in this study is a front bearing structure (FBS) which is part of the main load path on the engine. It faces different types of loading, mainly forces coming from engine bars and central tube and gas loads caused by air sucked into the engine. The FBS is a life limited part on the engine and should meet the number of cycles without any failure.

Main purpose of the study is to find out the number of cycles needed for definite crack lengths to appear on the FBS. To achieve this goal, it is taken advantage of the finite element modeling, commercial software, Ansys WB is used.

A previous study about FBS was already conducted and the historic models were developed in Ansys Classic. The strain levels seen under unit loads were checked with a few static tests and after some corrections model is validated. The first step of this study is conducted to see how close the results are between Ansys WB and Ansys. Two static structural models are developed and the results are checked. The difference between the tools is 0.8% in terms of total strain. Also, the difference for max equivalent stress is evaluated as 1.6%. The results show that the Ansys WB model is good enough to be used in fatigue and crack propagation analyses.

To predict life number of cycles, strain-life method is preferred since the loading is low cycle fatigue and the method takes into account the plastic strains. The strain life parameters are not easy to determine and find in literature for the specified material, Ti-6Al-4V. Therefore, the parameters are taken from a study based on Brinell hardness of the material. The loading is zero based and the Morrow correction is used in analysis. The number of cycles predicted is nearly 11000 cycles.

Furthermore, if the component is flawless, it is expected to have the crack where the max principal stress is observed. But in fatigue test, the first crack is observed on a different vane. Hence, before starting crack propagation runs crack location is changed due to test results. A series of analyses is conducted to evaluate the K_I and J-integral values at the crack tip edges. To model the crack on the geometry, a

parameter (crack length) is introduced. The vane has hollow structure which requires to prepare different FE models for different intervals of crack length. The FE models are run for these crack lengths and the results are extracted from 4 different paths which are vane edges. Path-1 where the max stress intensity factor, K_I is observed is selected. After showing K_{II} and K_{III} is not effective as K_I, with respect to the stress intensity factors on selected path, a polynomial curve is fitted to define ΔK which is essentially a function of crack length, a. After finding ΔK, to achieve the numbers of cycles needed, it is benefitted from Paris-Erdogan's Law. Also prior to these calculations, the J-integral values have been evaluated to show that the crack growth is in Region-2 by showing the values are below the critical J-integral value.

The fatigue behavior of the part is monitor with an LCF fatigue test and all data is stored. In Chapter 4, related test data and details of test rig is given.

Finally, J-integral values gathered from FE analysis showed the crack is always in Region-2. Also the test data shows a similar behavior in the mean of crack growth rate. Up to crack length reaches 20 millimeters, a difference between the analysis and the test results is observed, due the complexity of the geometry, unsymmetrical loading and assumed polynomial. To conclude, the numbers of cycles needed for crack growth from FE analysis and test data exhibits consistent results in Region-2 where the crack growth rate follows a linearly increased pattern.

REFERENCES

[1]   Boyce, M.P., *GasTurbine Engineering Handbook,* 2nd Ed., Gulf Professional Publishing, **2002.**

[2]   Eady, C., *Modes of Gas Turbine Component Life Consumption - Chapter4*, http://ftp.rta.nato.int/public/PubFulltext/RTO/TR/RTO-TR-028/TR-028-04.pdf (May, **2015**)

[3]   NESC Academy Webcast, *Metal Fatigue Part-1*, https://mediaex-server.larc.nasa.gov/Academy/Play/eb24e80551684a74838ab675cf9fd6be1d?catalog=aa34c90a-f143-46bc-8cd0-11a0d40da782 (May, **2013**).

[4]   Hosford, W.F., *Mechanical Behavior of Materials*, Cambridge University Press, **2005**.

[5]   Budynas R.G., Nisbett J.K., *Shigley's Mechanical Engineering Design*, 8th Ed., McGraw Hill, **2006**.

[6]   Meyers, M., Chawla, K., *Mechanical Behavior of Materials*, 2nd Ed., Cambridge University Press, **2009**.

[7]   ASM International, Fatigue - Chapter14, *Elements of Metallurgy and Engineering Alloys*, 243–265, **2008**.

[8]   Bishop, N.W.M., Sherratt, F., *Finite Element Based Fatigue Calculations,* NAFEMS, **2000**.

[9]   Basan, R., Rubeša, D., Franulović, M., Krian, B., A novel approach to the estimation of strain life fatigue parameters, *Procedia Engineering*, 2, 1, 417–426, **2010**.

[10]   Schijve, J., *Four Lectures on Fatigue Crack Growth*, Delft University of Technology - Department of Aerospace Engineering, Report LR-254, Delft, **1977**.

[11]   Patrıcio, M., Mattheij, R.M.M., *Crack propagation analysis*, CASA Report, Eindhoven, **2007**.

[12]   Suranaree University of Technology, *Fatigue of Metals - Chapter12,* http://eng.sut.ac.th/metal/images/stories/pdf/12_Fatigue_of_metals_1-32.pdf (May, **2015**)

[13]   Vardar, Ö., *Fracture Mechanics,* Bogazici University Publication, **1988**.

[14]   Gdoutos, E.E., *Fracture Mechanics An Introduction,* Kluwer Acamedic Publishers, **1993**.

[15]   Rao, S.S., *The Finite Element Method In Engineering,* 4th Ed., Elsevier Science & Technology Books, **2004**.

[16]   ANSYS Inc., *Ansys Online Help*, Ansys v.16, **2015**.

[17]   Carpinteri, A., Paggi, M., Are The Paris' Law Parameters Dependent On Each Other?, *Frattura ed Integrita Strutturale,* 2, 10-16, **2007**.

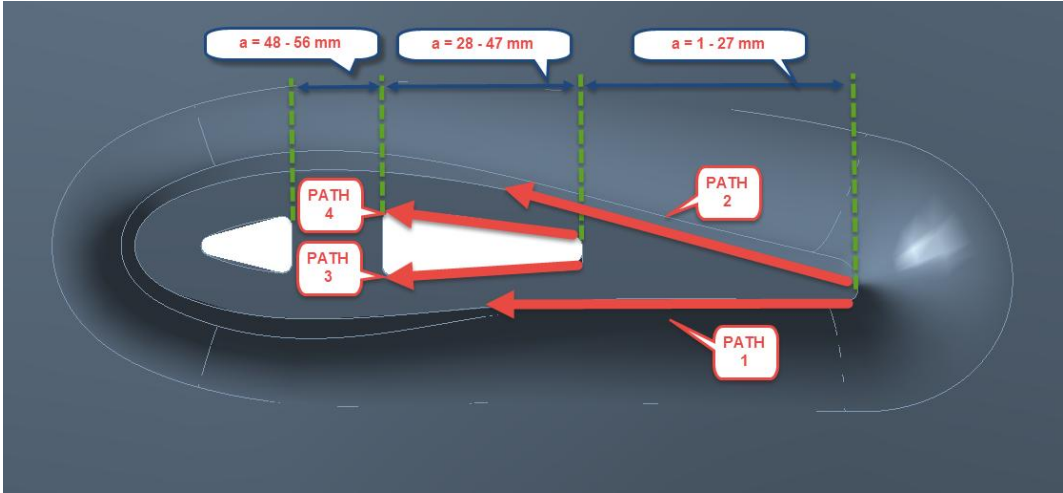# APPENDIX A - Path Definitions and Related Data

Fig A.1 Path Definitions

Table A.2 J-int [J/m²] through different paths

a [m]	J-integral [J/m²]			
	Path-1	Path-2	Path-3	Path-4
0,001	893,1	285,2	-	-
0,003	5559,7	2965,4	-	-
0,005	5799,9	1918,9	-	-
0,007	5806,2	1894,8	-	-
0,008	4473,2	3948,5	-	-
0,011	3832,4	3541,5	-	-
0,015	3224,4	3166,7	-	-
0,018	2959,6	2877,0	-	-
0,020	2942,7	3324,6	-	-
0,023	3143,3	2719,1	-	-
0,025	3787,5	1863,7	-	-
0,027	4958,7	1208,0	-	-
0,030	4761,3	1934,4	2542,7	4557,4
0,034	3164,2	1445,1	2722,5	5628,2
0,039	1096,0	792,3	2089,5	5336,9
0,042	1104,2	1157,2	1923,3	4870,5
0,047	298,4	593,3	2950,7	5259,7
0,051	156,7	768,0	-	-

1. Path-1
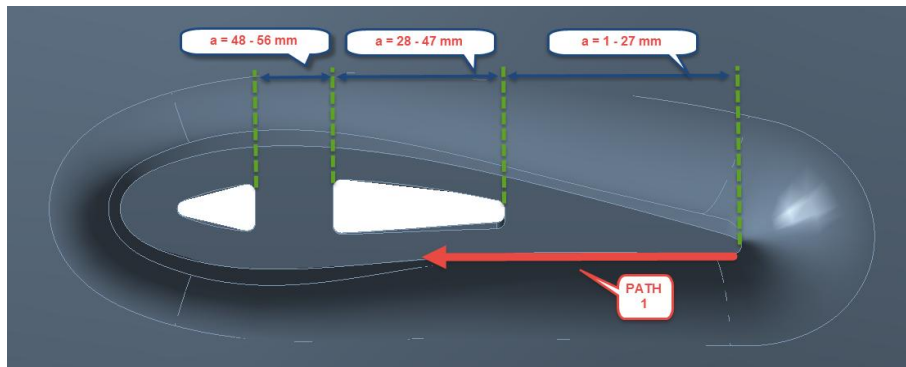
Fig A.2 Path Definition - 1

Table A.2 KI-KII-KIII [MPa·m^(0.5)] through Path-1

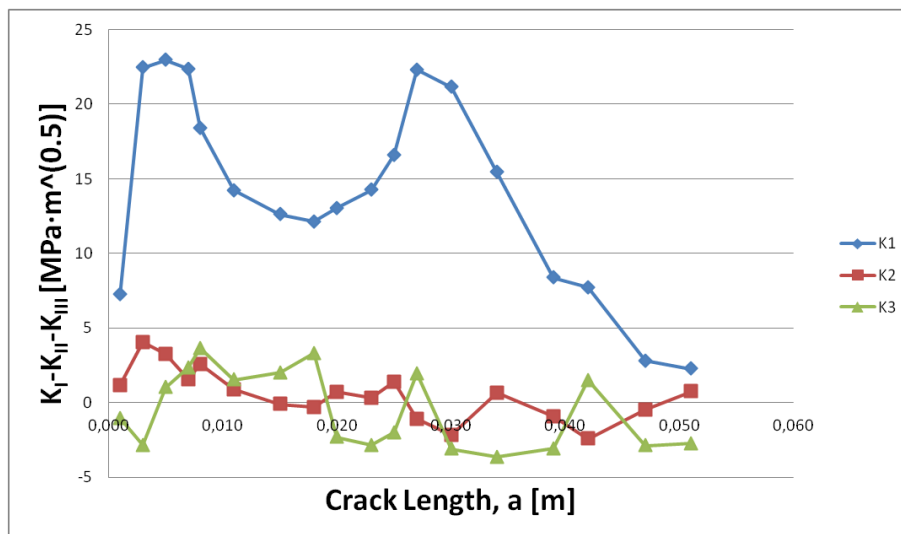| a [m]	K1	K2	K3
0,001	7,236	1,150	-1,031
0,003	22,438	4,025	-2,859
0,005	22,952	3,249	1,023
0,007	22,352	1,554	2,335
0,008	18,396	2,589	3,659
0,011	14,226	0,870	1,524
0,015	12,601	-0,111	2,012
0,018	12,111	-0,315	3,300
0,020	13,021	0,706	-2,328
0,023	14,242	0,318	-2,847
0,025	16,609	1,383	-2,012
0,027	22,307	-1,088	1,958
0,030	21,147	-2,187	-3,112
0,034	15,441	0,656	-3,651
0,039	8,370	-0,949	-3,084
0,042	7,723	-2,431	1,515
0,047	2,815	-0,474	-2,880
0,051	2,270	0,732	-2,736

Fig A.3 KI-KII-KIII [MPa·m^(0.5)] vs a [m] for Path-1

67
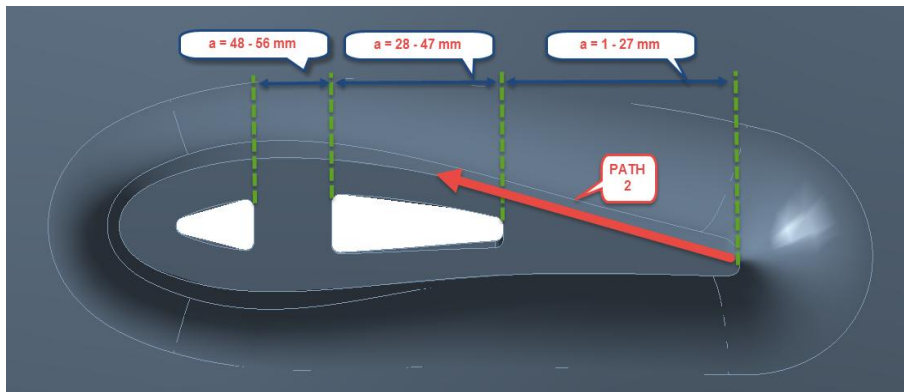
2. Path-2

Fig A.4 Path Definition - 2

Table A.3 KI-KII-KIII [MPa·m^(0.5)] through Path-2

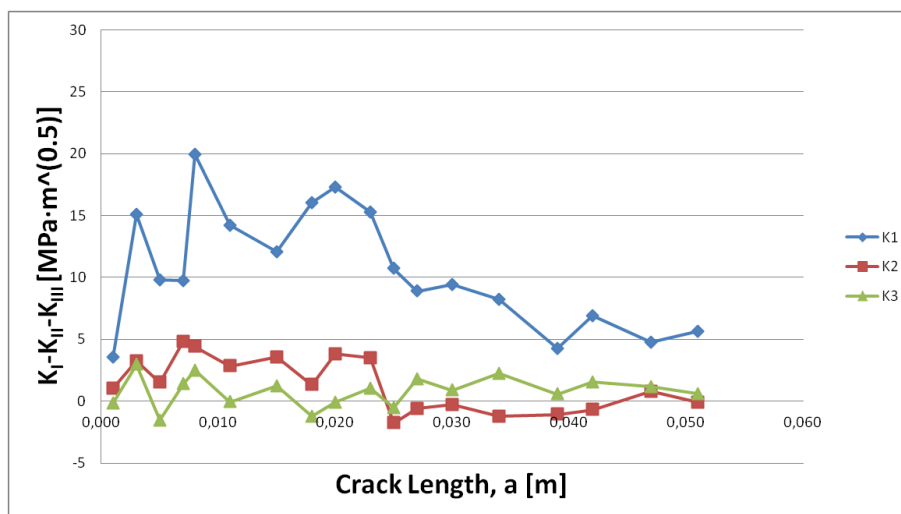| a [m]	K1	K2	K3
0,001	3,554	1,022	-0,150
0,003	15,103	3,239	2,965
0,005	9,790	1,514	-1,538
0,007	9,739	4,832	1,385
0,008	19,948	4,420	2,489
0,011	14,226	2,843	-0,056
0,015	12,087	3,561	1,212
0,018	16,044	1,336	-1,235
0,020	17,308	3,825	-0,091
0,023	15,279	3,520	1,053
0,025	10,717	-1,756	-0,523
0,027	8,893	-0,614	1,816
0,030	9,399	-0,290	0,892
0,034	8,219	-1,241	2,264
0,039	4,256	-1,070	0,568
0,042	6,917	-0,680	1,568
0,047	4,747	0,783	1,149
0,051	5,638	-0,106	0,587

Fig A.5 KI-KII-KIII [MPa·m^(0.5)] vs a [m] for Path-2

68
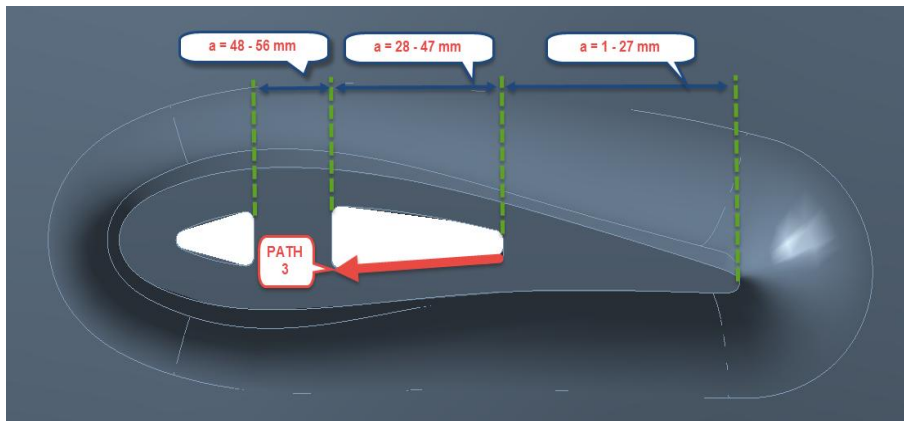
3. Path-3

Fig A.6 Path Definition - 3

Table A.4 KI-KII-KIII [MPa·m^(0.5)] through Path-3

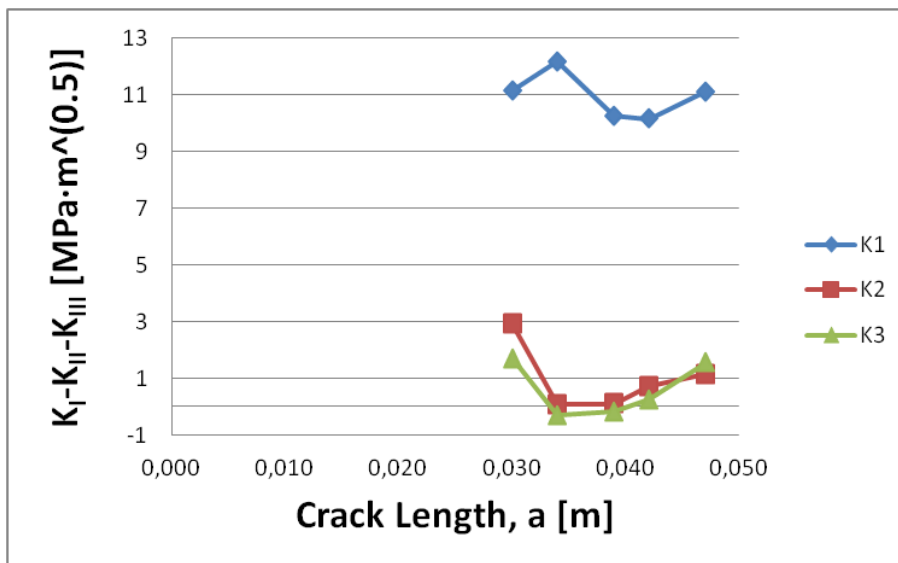| a [m]	K1	K2	K3
0,030	11,140	2,905	1,684
0,034	12,149	0,072	-0,312
0,039	10,250	0,106	-0,185
0,042	10,141	0,723	0,234
0,047	11,083	1,159	1,547

Fig A.7 KI-KII-KIII [MPa·m^(0.5)] vs a [m] for Path-3

4. Path-4
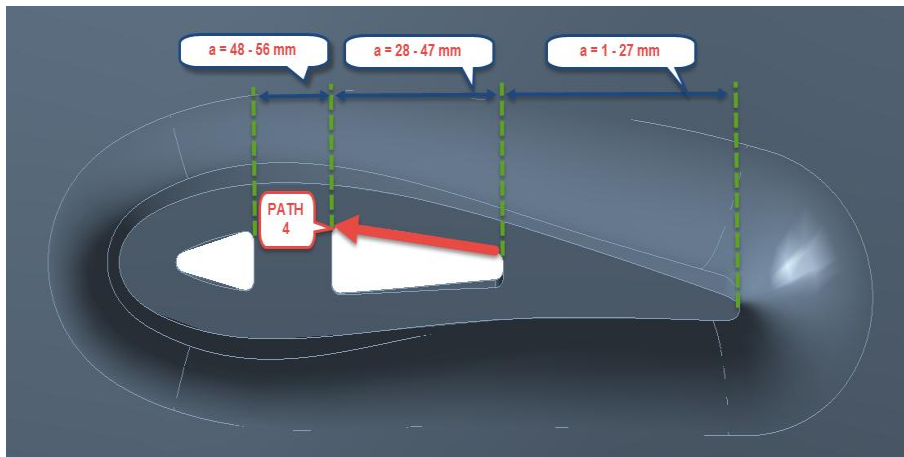
Fig A.8 Path Definition - 4

Table A.5 KI-KII-KIII [MPa·m^(0.5)] through Path-4

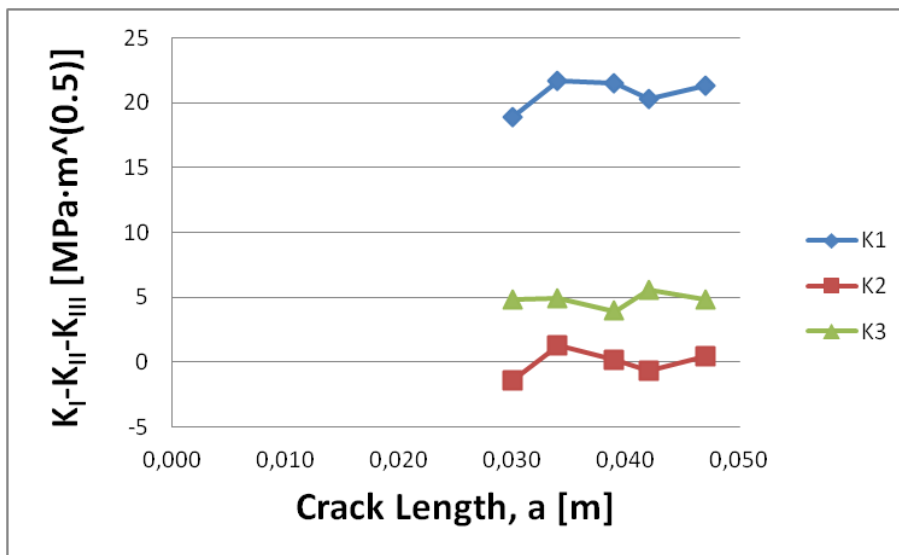| a [m]	K1	K2	K3
0,030	18,895	-1,410	4,790
0,034	21,678	1,267	4,889
0,039	21,489	0,154	3,923
0,042	20,240	-0,705	5,589
0,047	21,289	0,449	4,788

Fig A.9 KI-KII-KIII [MPa·m^(0.5)] vs a [m] for Path-4

70

CURRICULUM VITAE

Credentials

Name, Surname : Ayşegül Yamaner

Place of Birth : Konya / TURKEY

Marital Status : Single

E-mail : yamaneraysegul@gmail.com

Address : Yenişehir Dt. Bıkmaz St. No:2/6 D:4 Pendik/İSTANBUL

Education

High School : Konya Meram Anatolian High School

BSc. : Hacettepe University - Mechanical Enginnering Department

MSc. : Hacettepe University - Mechanical Enginnering Department

PhD. : -

Foreign Languages

English : Advanced

German : Intermediate

Work Experience

Turkey Technology Center (GE Aviation - TEI) - (2013 - 2015)

Tusas Engine Industries (TEI) - (2011 - 2013)

Areas of Experience

Finite Element Modeling, Structural Design, Stress Analysis (Rotating/Structural)

Projects and Budgets

-

Publications

-

Oral and Poster Presentations

-